The Design and Testing of a Biologically Inspired Underwater Robotic Mechanism

by

Michael Sachinis

Submitted to the Department of Mechanical Engineering
in partial fulfillment of the requirements for the degree of

Master of Science in Mechanical Engineering

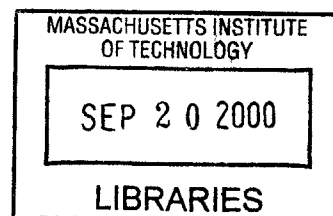at the

MASSACHUSETTS INSTITUTE OF TECHNOLOGY

June 2000

Author . . . .
Department of Mechanical Engineering
May 8, 2000

Certified by . . . .
Michael S. Triantafyllou
Professor, MIT
Thesis Supervisor

Read by . . . .
David L. Trumper
Professor, MIT
Thesis Reader

Accepted by . . . .
Ain A. Sonin
Chairman, Department Committee on Graduate Students

The Design and Testing of a Biologically Inspired Underwater Robotic Mechanism

by

Michael Sachinis

Submitted to the Department of Mechanical Engineering
on May 8, 2000, in partial fulfillment of the
requirements for the degree of
Master of Science in Mechanical Engineering

Abstract

This thesis describes the design, construction and testing of the new generation Robo-tuna, a laboratory six-joint robotic mechanism intended to imitate the motion and function of a real size bluefin tuna. Attached to a towing carriage in the MIT Testing Tank Facility, this mechanism was designed as an improved form and substitute of the original robot, built in 1993. Major issues of design as well as performance results from its four-month life are discussed in detail. Finally, the issue of flow sensing around its flexible hull is addressed and first steps towards this implementation are described.

Thesis Supervisor: Michael S. Triantafyllou
Title: Professor, MIT

Acknowledgments

I would first like to express my sincere gratitude towards my advisor, Prof. Michael Triantafyllou, and towards Dr. Franz Hover for the unlimited guidance and support they have offered me, for supervising my thesis and for giving me the opportunity to work in a great engineering environment.

Special thanks also go to Prof. D. Trumper for being extremely accommodating and taking the time to read my thesis, and to Ms. Regan for her remarkable patience.

My extended gratitude also goes to Fred Cote who patiently guided me in paths of engineering that I had never explored before, who never complained when I broke or borrowed tools and who taught me the value of persistence in machining. I hope the days of polypropylene tubing will one day be remembered as a nice memory.

I would also like to thank all the graduate and undergraduate students working in the Towing Tank, for transforming a dark underground laboratory to such a nice working environment, even during long nights of stressful work. Special thanks go to David Beal, with whom I worked very closely on the Robotuna project, and whose guidance and good humor made it more enjoyable and certainly more educational. I am confident that he will take good care of the Robotuna, and I wish that the Robotuna will reward him with good results in the future. Special thanks also go to Michael Jakuba, Katherine Reid and Kate Thompson for taking a large part of the Robotuna's weight on their backs and for doing such a great and professional work.

MIT would not have been such a fun place without the presence of a certain group of Mediterranean people. I wish them all good luck in their studies and work and expect to see them soon in a warmer place.

My deep gratitude also goes to my parents for their unlimited love and support and for so many years of sacrifice towards my education, to my brother for he has been a source of great encouragement, and to my uncle Harry for truly being a second parent. Most importantly, I would like to thank my stepfather, George, for believing in me and offering me opportunities that would have only been a dream without him. If I made it to MIT, it is mostly because of him.

Finally, I wish to thank Mayssam for being a true pillar of support, comfort, guidance and happiness at MIT. She has helped me in unimaginative ways. I hope these will be more than memories of the past. She has made it extremely difficult for me to leave MIT, and has encouraged me tremendously to return.

Contents

List of Figures

9

List of Tables

Chapter 1

Introduction

The original Robotuna was designed and built in the MIT Ocean Engineering Testing Tank Facility in 1993, as a response to the need for highly maneuverable underwater vehicles of greater autonomy in oceanographic and military applications. The design of the Robotuna, conceived by graduate student David Barrett, was an attempt to imitate the biological shape form and motion of a medium sized bluefin tuna. This decision was based on the popular notion in the robotics community that nature has solved the issue of propulsion through evolution of its species and should therefore be a major source of study and inspiration for man-made propulsion systems. Thus, studying the motion of such an advanced swimmer that can cross oceans in the course of days and can allegedly produce instantaneous speeds up to 50 miles per hour, seemed like a logical start.

Inside its tuna-like body, the Robotuna consisted of a cable-driven robotic arm of six degrees of freedom that was rigidly connected to an overhanging carriage by means of a surface-piercing hydrofoil mast. The depth was thus constrained and the robotic mechanism was allowed to swim in straight paths only. Furthermore, the rigid connection to the carriage allowed all instruments and motors to be positioned in a dry and spacious environment.

During its first years of operation, the Robotuna participated in a large number of experiments that were targeted towards the development of an optimally efficient swimming style by means of a genetic algorithm approach. Moreover, dye injection

and laser visualization techniques were applied repeatedly in an effort to shed light to the mysteries of efficient fish swimming.

More than five years after its construction, it was apparent that the Robotuna had aged significantly and was unable to produce the performance levels that were reported in its early history. Furthermore, many of its mechanical parts had shown distinct signs of corrosion and decay, as they had far exceeded their intended design life of a few months. As a consequence, most measurements that were critical in the performance evaluation were deemed to be unreliable and imposed a halt to the testing process. Efforts were subsequently made by graduate student Sam Tolkoff to replace certain parts of the tuna and proceed in a partial restoration, but they marked only limited success [16].

Assessing the level of degradation based on Tolkoff's inspection analysis and adhering to the desire for a more advanced Robotuna with extended capabilities, it was decided that the second generation of tuna should be developed. The task was undertaken by graduate student David Beal and the author in the spring of 1999. This called for the design and construction of an entirely new swimming mechanism that could produce satisfactory performance levels, increase the reliability of position and force sensor outputs and ultimately possess higher "intelligence" capabilities by detecting the characteristics of its surrounding flow and responding accordingly to maximize its thrust or efficiency.

This effort has been under way for one year and while the new Robotuna has been swimming smoothly for nearly four months, the project is still far from its final conclusion. In this thesis, the author offers a detailed description of certain design aspects of the new Robotuna where he was primarily involved in. Some of the relevant work of graduate student David Beal and undergraduate students Michael Jakuba, Katherine Reid and Kate Thompson is also mentioned briefly for the purpose of completeness and in order to portray a more clear picture of the overall robotic mechanism. Issues relating to the general architecture of the model are discussed extensively with emphasis on the principles behind the actuation system design, and some evaluation based on primary results has been attempted. Initial performance

13

results, based on an early set of genetic algorithms, are mentioned and backed with suggestions and recommendations for the future. In a later chapter, the idea of further "intelligence" capability is introduced and the design of an artificial lateral line sensor array as well as a large scale vorticity production mechanism are described and evaluated.

It is hoped that this piece of writing may stand as an accurate report of what has transpired in the early stages of life of the new Robotuna, and may be a useful means of pointing out the strengths and weaknesses of the mechanism, so that improvements will be made in the near future and the main goal of the investigation will be fulfilled.

Chapter 2

Design Aspects of the New Robotuna

2.1 Design Philosophy

The design of the new Robotuna was based on the principles of Barrett's fish. The simplicity of Barrett's mechanism and its success in imitating the undulating motion of a cruising tuna suggested that the new generation should by an improved offspring of the original version rather than a complete stranger to it [1]. Furthermore, by keeping the design philosophy unchanged, it would be easier to tackle specific problems and limitations that were identified in the old tuna, especially towards the late stages of its life. Finally, by adopting a similar structure and testing methodology, we would be allowed to make more accurate comparisons between the two generations.

Like Barrett's fish, the new Robotuna was designed as a test bed for an efficient, straight line swimmer. Combining efficient cruising with swift maneuvering capabilities is a task kept for future generations. Consequently, it was decided that autonomy was not required yet and the new mechanism could still be supported by an overhanging carriage that would provide depth control, and at the same time level the fish and host the powerful motors that actuate it as well as most of the necessary electronics. This decision simplified the design considerably and offered valuable space that was desperately needed, especially near the tail section. Moreover, it reduced

the dynamics of the overall system to that of an extended arm linkage mechanism that could swing in the horizontal plane only, with a total degree of freedom equal to the number of independent joints.

Having preserved these fundamental aspects of the old tuna mechanism, David Beal and the author defined our new design philosophy to target four areas that required change or offered room for further improvement. The first one involved the addition of new external features to the body, so that the Robotuna would follow more faithfully the shape of a real bluefin tuna. It was considered that details in the shape that were ignored in the first model might be responsible for secondary hydrodynamic effects worthy of investigation and, in some instances, could even facilitate the design. A notable example to be discussed later in detail involved the presence of an expanded lateral keel near the caudal peduncle of the fish.

The second area of attention involved the construction of a smoother external surface. The intent was twofold and aimed towards improving DPIV visualization conditions as well as reducing flow disturbances around the fish. Since the Robotuna is designed to operate at a near transitional Reynolds number, large irregularities in the surface might affect significantly the flow and even cause separation. This would easily increase the level of hydrodynamic resistance and could seriously inhibit the tuna's ability to use vorticity control for drag reduction.

Thirdly, the design of the new Robotuna was sensitive to the addition of flow-measuring sensors. Such sensors were expected to play the role of a lateral line in a fish, giving us the capability of detecting the flow around the Robotuna through pressure measurements. It was hoped that this knowledge could eventually be used both to investigate the details of fish swimming and also to provide the sensor output in a real-time feedback controller that would optimize the swimming parameters.

Finally, most of the weight of the design was placed at improving the precision of the transmission mechanism. A novel transmission system was required that would be devoid of large levels of uncertainty and any kind of nonlinearity. This was recognized to be extremely important for the understanding of the physics of fish swimming. Vorticity control is an unsteady phenomenon and, consequently, the search for high
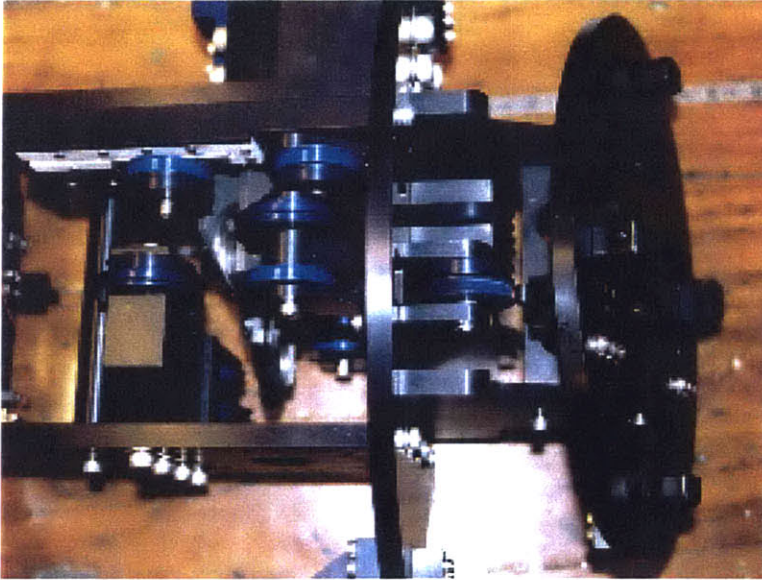
Figure 2-1: A close look to the passive joint connecting the plate of the nosecone to the main body of the Robotuna.

propulsive efficiency is to a large extent a problem of synchronization between the main body of the fish and its tail. Position errors in the joints were therefore deemed highly undesirable and had to be reduced to an acceptable level of less than one degree. This effort is described below in detail and relies both on a novel transmission mechanism and the installation of accurate position sensors on the individual joints.

2.2 Actuation Considerations

2.2.1 Competing Systems of Actuation

The new Robotuna is actuated by means of a cable drive system. Aircraft-steel cables, $\frac{1}{16}$ inches in diameter originate from the drums of the motors and fan out to the active joints of the structure. Overall, there are six joints that correspond to separate links of the structure, but only five are active. The sixth one controls the action of the nose section and is mechanically connected to the first active joint to perform an anti-clastic movement, similar to that observed in real tunas[1].

This passivity is imposed for reasons of simplicity, as it is thought that the ac-

17
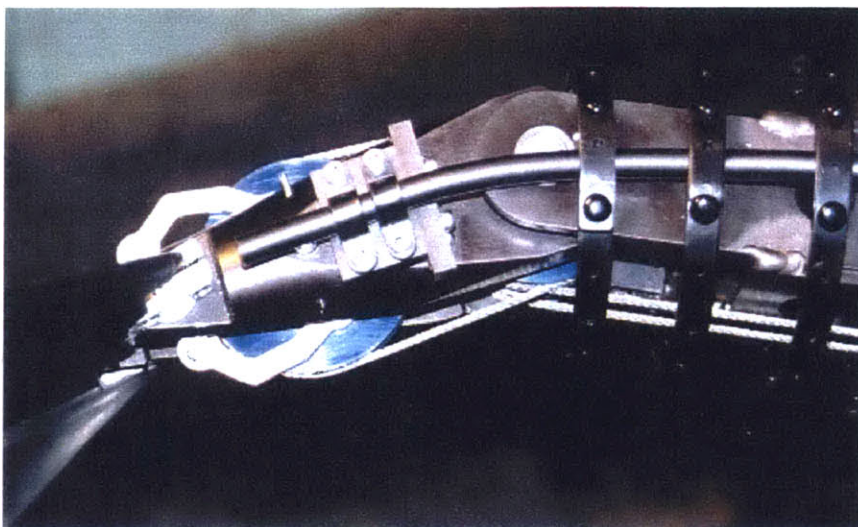
Figure 2-2: Detailed view of the tail end of the Robotuna, showing the large peduncular link that supports the lateral keel mechanism.

curacy in the curvature of the nose is not as critical as the curvature of the main body [1]. The spacing of the joints decreases away from the nose and towards the tail, in a manner similar to Barrett's arbitrarily imposed "cosine rule" [1]. Near the caudal peduncle however, this cosine rule deviates and the spacing increases. This is effectively achieved by omitting the second to the last joint and producing a strong and massive peduncle, without compromising the flexibility of the tuna's undulatory motion. From a structural point of view, this modification is highly desirable because it allows the strengthening of the skeleton at a very critical point. Moreover, it provides the necessary space for the installation of a fixed lateral keel.

Had the lateral keel been pivoted on a moving joint, its design would have been significantly more complicated and most likely would have affected negatively the smoothness of the outer surface.

In the early part of the design of the new Robotuna, the cable drive system of actuation was challenged by several other alternatives. The most important of these competitors included a hydraulic network and a bar-linkage system, the latter being conceptually similar to the one used to connect the wheels of old locomotives.

Hydraulic actuation provides compactness and strength, but introduces significant
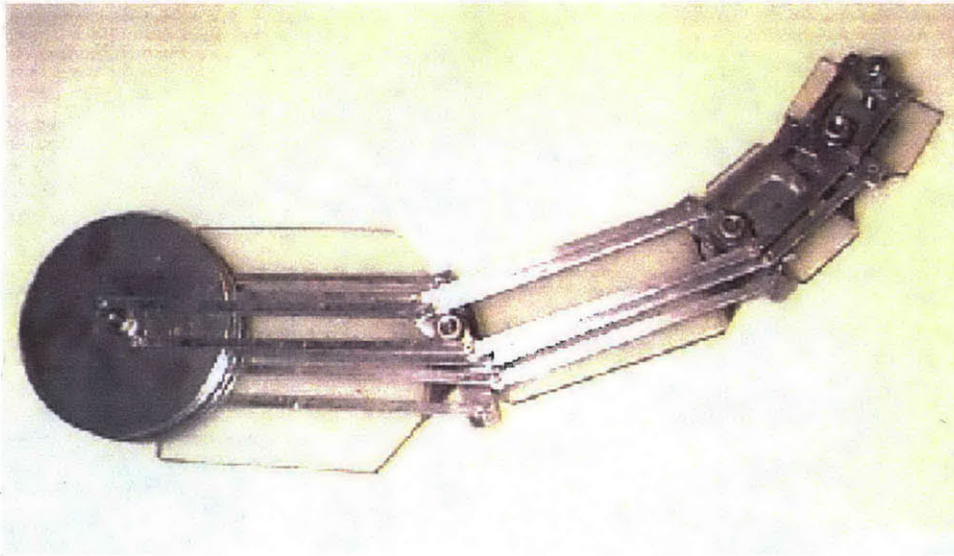
Figure 2-3: General view of the bar-linkage system, as it was conceived in the early stages of the design of the Robotuna.

complexity and cost that the designers were not willing to undertake. Furthermore, it reduces significantly the mechanical efficiency of the system, thereby requiring motors with larger power capabilities.

A bar-linkage inter-connection can offer three different but nonetheless significant benefits: **simplicity, linearity** and **perfect coupling**. The simplicity stems from the fact that the system can be set up almost in its entirety by mechanically connecting only two types of building blocks, aluminum pulleys and steel rods. By properly pinning the rods on the pulleys so that they are always arranged in parallel pairs, as shown in Figure 2-3, one can achieve perfect coupling of the joints. This means that the actuating motor of each joint can only affect the global orientation of the link directly attached to it. This is a highly desirable characteristic since it reduces significantly the overall angular error in the rear joints, and especially in the tail. In the opposite situation of perfect uncoupling, the total position error at a joint is the sum of the uncertainty of that joint and what is accumulated from all preceding ones. Evidently, even a small error of the order of one degree on each joint implies that the position of the tail can deviate by as much as five degrees, which is unacceptably high for our standards. Pure coupling resolves this problem and keeps the

19

total error within the uncertainty of each individual joint. Furthermore, this type of arrangement guarantees that the relation between the motor-drum's angle and the angle of each link referenced to a global fixed frame is perfectly linear. Linearity is very important because it greatly simplifies the position commands and presents a more accurate picture of the tuna's motion.

The bar-linkage inter-connection system however, is severely limited in four ways. Firstly, it introduces a great deal of frictional losses to the mechanism, by requiring ball bearings at each pinning location. Secondly, the bars are most likely to be weaker than steel cables and can potentially buckle when large compressive stresses are applied to them. Moreover, they are expected to undergo some twisting or bending deformation, thus affecting the accuracy of the mechanism. Finally, the most serious limitation rises from the fact that the tension applied to the bars can be shown to be inversely proportional to the cosine of the joint's absolute angle. This is necessary in order to keep the bar couples parallel to each other and preserve linearity and perfect coupling. Even though the relative angles of the links are not expected to exceed 30 degrees, the absolute angles could easily approach 90 degrees, thus increasing tensile and compressive stresses to dangerously high levels. This can be shown in Figure 2-3, where the last joint is nearly aligned to the previous one and yet the first couple of bars that are associated with it experience high stresses.

The weight of these limitations pushed the design towards a cable-driven actuation system. The latter is conceptually closer to the tendon drive actuation used by real fish, and simultaneously offers simplicity, accessibility, low cost and high strength that cannot be surpassed by any of the other alternatives [1]. The arrangement of this cable drive system however, differs significantly from the one used in Barrett's tuna and attempts to adopt the benefits of the bar-linkage inter-connection, by imitating its main principle of operation.

2.2.2 Tendon Drive System

The particulars of the cable drive system will not be discussed in full detail. The interested reader may refer to Barrett's Master thesis for a more complete analysis

20

on this matter [1]. Instead, the discussion will be limited to three main "tricks" that have been employed to improve the actuation system according to the design goals specified in the previous section. These tricks are associated with an extended **idler pulley mechanism**, a novel **tail bar-linkage unit** and an alternative **compound pulley system**.

Extended Idler Mechanism

An essential component of the cable drive transmission mechanism is the idler pulleys that hold the cables together and direct them to their paths. In the original Robotuna there was a particular type of idler pulleys, termed by Barrett as "conduit idler pulleys" [1]. They consisted of a set of overlapping discs that embraced the cables and arranged them neatly in parallel planes along the centerline of the tuna. The major benefit of this design was that it confined and protected all cable paths to the center. Moreover, it was intended to produce perfect decoupling of the joints. This however was not achieved in reality. Simple trigonometry can show that perfect decoupling can occur only in the limit as the conduit idlers have vanishingly small radius and infinite curvature. In essence, this would correspond to sharp corners in the cable lines along the joints. Unfortunately, cable-wear regulations require that the radius of curvature stays above a certain minimum, which depends on the cable thickness. Consequently, the conduit idlers could not be made arbitrarily small, and a finite amount of coupling was inevitable. To make matters worse, this type of coupling was found to be a very complex nonlinear function of the size of the driving pulleys and the range of travel, with a noticeable effect on the joint angles. For example, the arrangement of the last two joints in the old Robotuna can be shown in Figure 2-4 to produce an error of approximately 15% in the tail angle. This does not include the accumulated error from the previous joints.

A solution to this problem was found by considering the case of bar-linkage actuation. Instead of concentrating the cables to the centerline of the fish, large idler pulleys were used that wrapped the cables perimetrically around them and spread the cable lines outward, towards the sides of the hull. Figure 2-2 shows the driving
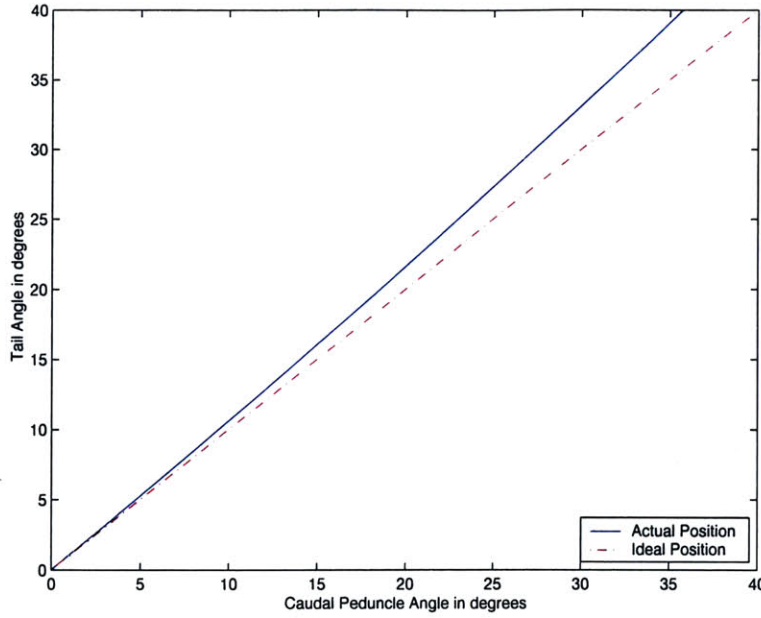
Figure 2-4: Actual angular position of the tail joint as a function of the previous joint angle alone. The deviation from the dotted red line shows imperfect coupling.

pulley of the lateral keel and its first idler (half-hidden). The cables are completely exterior to the main skeleton and only interior to the ribs. Once again, trigonometry can easily show two remarkable benefits. Firstly, linearity is always preserved while always operating safely above the minimum radius of curvature. Secondly, the degree of coupling can be found to depend linearly on the relative size between the driving and idler pulleys, marked by R and r respectively in the simple relation shown below. In this relation, γ represents the global (absolute) angle of the link, while θ stands for the global angle of the preceding link. When the two radii are set equal, the joints are perfectly coupled and the motion of the link does not affect the orientation of the following ones in absolute coordinates. At the other (impractical) extreme, when the idler pulleys have a vanishingly small size, the fully decoupled condition is recovered. A schematic demonstration of these two cases is shown in Figure 2-5.

$$\gamma = (1 - \frac{r}{R})\theta$$

For reasons of simplicity and reduction of error propagation to the latter joints, it was generally desired to keep the driving and idler pulleys at the same size. This

NEW ROBOTUNA
TRANSMISSION SYSTEM
DESIGN

OLD ROBOTUNA
TRANSMISSION SYSTEM
DESIGN
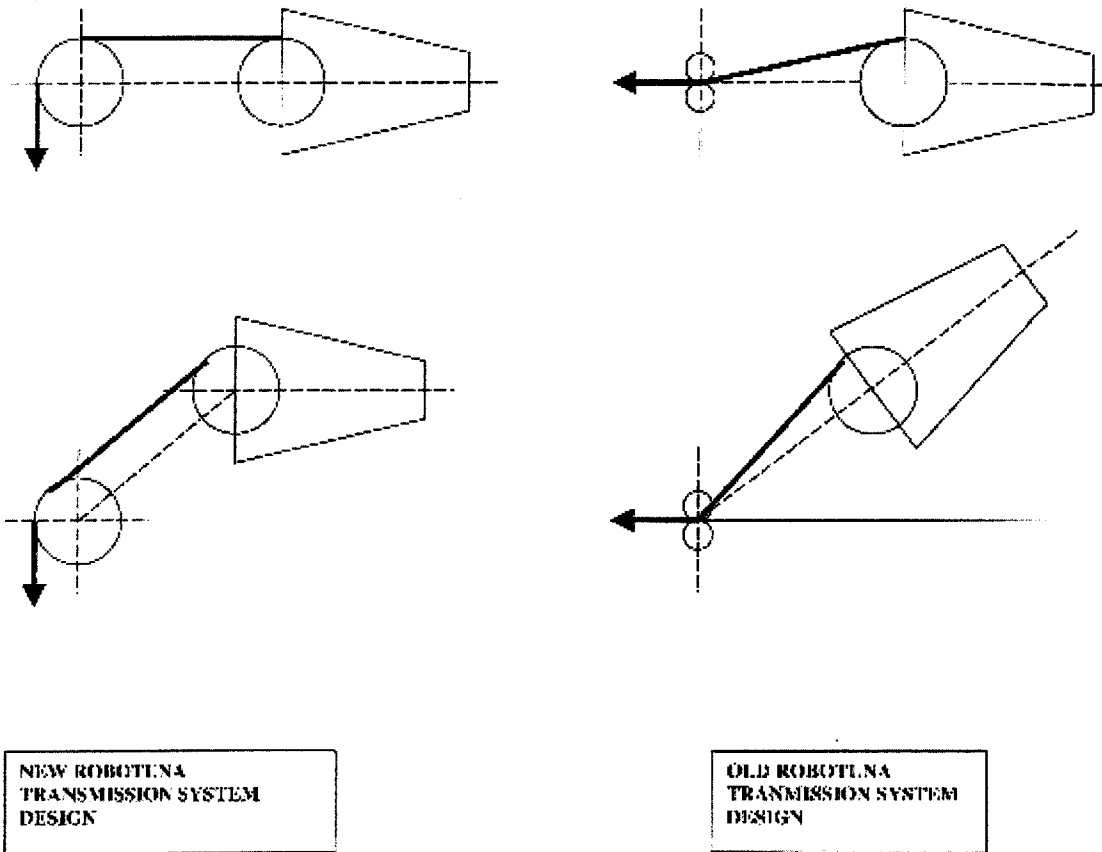
Figure 2-5: A schematic description of the fundamental difference in the idler pulley arrangement between the new and the old Robotuna. In the new Robotuna design, the rotation of a link leaves the orientation of the next link unaffected (perfect coupling). This is not the case with the old design, where the next link is expected to rotate by an equal amount (decoupling).

however was not always feasible, due to spatial limitations and cable stress considerations. Near the tail region, the cross-sectional area of the Robotuna decreases dramatically in order to comply with the slender and hydrodynamically fit shape of the fish. From a design perspective, packing all the necessary actuation and sensor components becomes a significant challenge. It may in fact appear to be tempting to keep the driving pulleys and idlers as small as possible. The consequence of this however is to increase the stress level at the cables, thus making cable compliance a real issue and a potential source of error. Different pulley sizes could yield more desirable solutions, and cost functions were constructed and optimized mathematically to investigate this possibility. These functions represented quadratic measures of the total angular error of a joint, which reflected the contribution of cable elongation and error accumulation from the previous (decoupled) joints.

For instance, the cost function for joint 4 had the form:

$$f = (\Delta\alpha)^2 + (1 - \frac{r}{R})^2(\Delta\alpha_o)^2$$

where

$$\Delta\alpha = \frac{\tau}{2kR^2}$$
$$\Delta\alpha_o = \frac{\tau_o}{2kR_o^2}$$

The constants τ, R, τ_o, R_o represent the maximum torque loads and driving pulley sizes relevant to the joint in question and the previous one. Figure 2-6 shows a plot of this cost function with the size of the driving-pulley for joint 4 (placed at the lateral keel). Different curves correspond to different driving-pulley sizes for the previous joint.

Tail bar-linkage unit

The area near the caudal peduncle of the tuna contains a feature which was given special attention. In biological terms, it is called "lateral keel" and represents a wide, disc shaped bony keel which extends horizontally along the sides of the fish[11] Its noticeable size and effect on the external geometry suggest that it might have
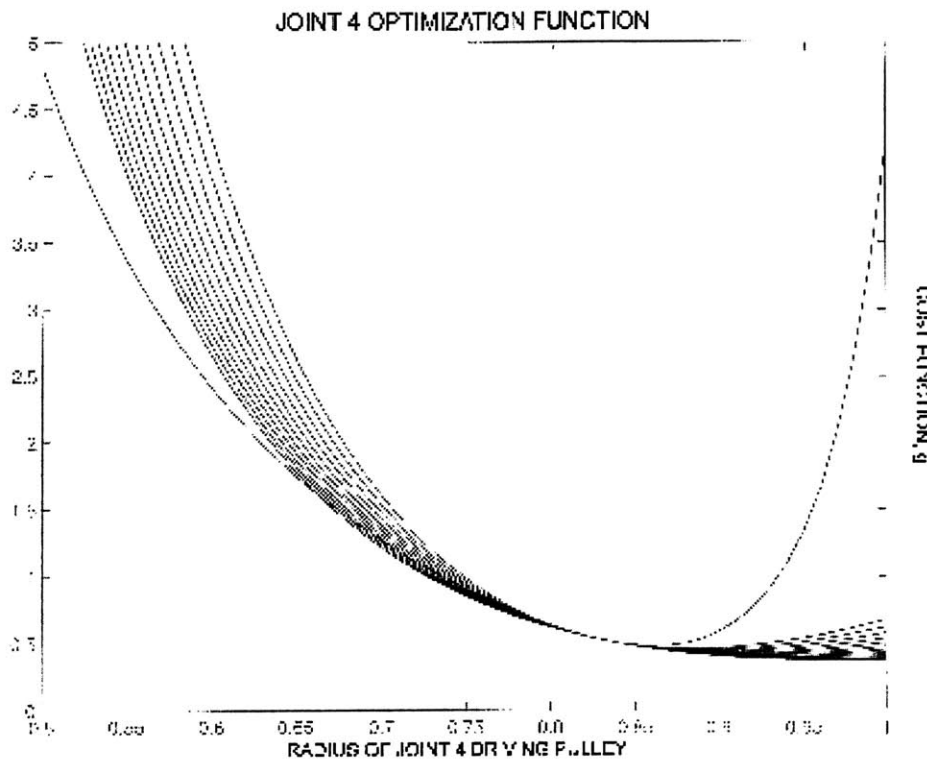
Figure 2-6: Cost function used for the minimization of the angular uncertainty in joint 4.

a valuable hydrodynamic contribution, perhaps by reducing the added mass in the sway direction near the peduncle, and hence the power that is necessary to swing the tail. More importantly however, it is thought that its primary function is purely mechanical and provides a biological pulley mechanism that increases the contact angle between the great lateral tendons and the hypural plate, thereby increasing the amount of available torque (see Figure 2-7).[4]

The modeling of the lateral keel was very desirable when designing the new Robotuna, because it introduced some needed space and allowed for the possibility of further strengthening the tail. To accomplish the latter, nature was used again as a source of inspiration. A large driving pulley was located in the position of the lateral keel as shown in Figure 2-2, resulting in an increase in available torque, similar to the one described above. The location of this pulley was inconveniently far away from the tail foil however and required a 1.5 inch extension in the transmission. A bar linkage system of the type described in the previous section was the optimal candidate so-
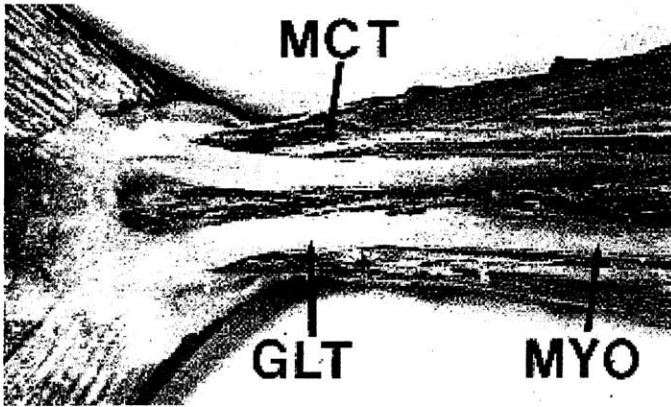
Figure 2-7: Side view of the lateral keel section in a real tuna. Courtesy of M.W.Westneat et al.[11] . Though the disc-shaped form is not clearly shown, the curving of the great lateral tendons (GLT) is obvious.

lution for this problem, primarily because it avoided the necessity of a separate loop of cables and guaranteed robustness and rigidity. Moreover, it saved some valuable space for the placement of position sensors and perhaps even for pressure sensors.

Each of the two bars of the system featured two sharp bends which are evident in Figure 2-2. These bends ensured that there would be no contact with the vertical tail shaft and thus helped to increase considerably the tail's range of motion. Despite their highly irregular shape however, they moved in parallel to each other as imposed by coupling and linearity requirements. Their rectangular cross-section was optimized to fit in the constricted geometry and provide very high axial and flexural rigidity.

Finally, the bars were pinned to the large driving pulley and the tail connector (which was an equivalent hypural plate for the mechanical tuna) by means of minia-ture, double-sealed stainless ball bearings of low wear.

The overall caudal peduncle and tail mechanism resulted in a strong tail with minimal joint errors, which could be accurately controlled in a linear manner. This was an important step towards the development of a reliable Robotuna that can be used to investigate the details of fish-swimming. Ideally, position sensors would be necessary to identify precisely the exact orientation of the links and perhaps even to provide a closed loop control mechanism for perfect tracking. The placement of such sensors has been considered in the design and will be discussed later in more
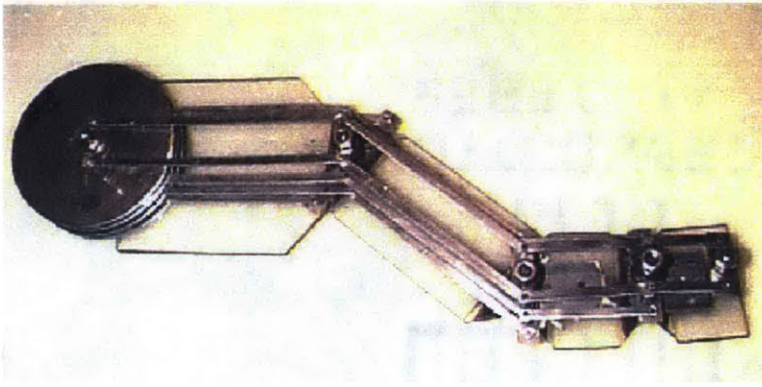
Figure 2-8: Demonstration of perfect coupling principle in the case of a bar-linkage actuation system. The rotation of the second link leaves the following links at the same orientation.

detail. Nevertheless, even without these sensors, visual observations and high thrust production measurements with the new Robotuna seem to indicate that the tail indeed performs as commanded.

Compound Pulley System

Another fundamental characteristic of the transmission design for the new Robotuna is related to the compound pulley system mechanisms that control the motion of the first two links. The idea behind a compound system was borrowed from Barrett's original tuna and is based on the need to reduce the torque required by the driving motors [2]. The first few joints are expected to withstand larger torques than the later joints, due to their relative distance from the tail foil, a fact which is particularly apparent in the old Robotuna design and has been verified by power measurements. The partial coupling of the new design alleviates some of the power requirement from the leading joints by distributing the load more uniformly between the motors, but is not sufficient to reduce the necessary torque to a satisfactorily low level. The latter however can be traded for a greater angular velocity requirement. This is a desirable step in order to comply with the specifications of the motors.

As in the original Robotuna, the compound systems consist of a combination of two pairs of pulleys that are fixed on different bulkheads. The effect is to reduce
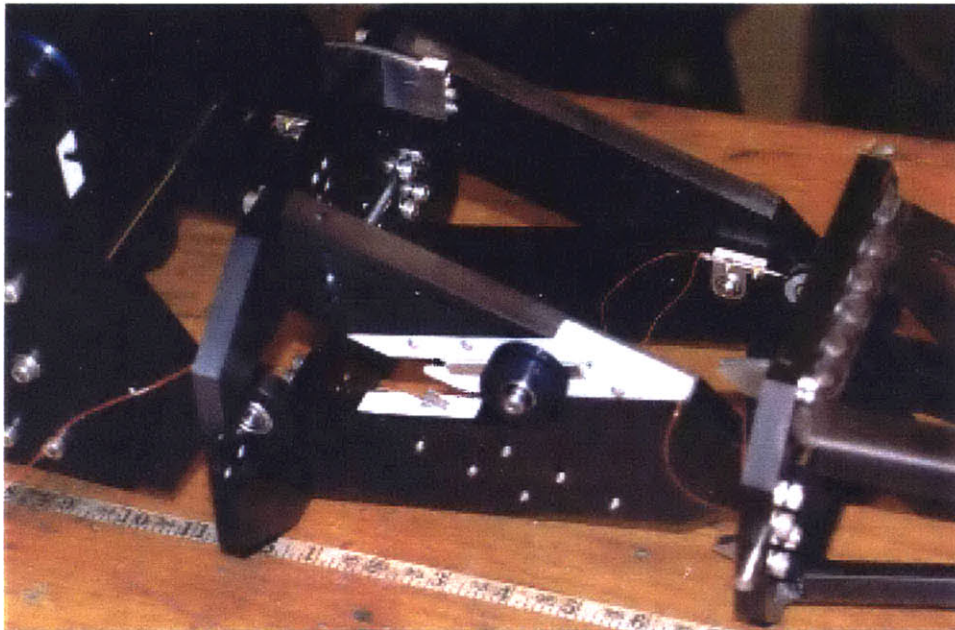
Figure 2-9: Closeup view of the compound-pulley configuration as was implemented in the case of joint 1. A pair of blue pulleys is allowed to slide along the white delrin channel. In reality, this pair is cable connected to a second pair (not shown) axially located on the left joint. Finally, a short cable (not shown) connects the sliding pulleys to the side of the bulkhead of the right joint.

the cable tension by a factor of four and increase the angular velocity of the motor drums by the same factor. The idea behind this mechanism is very welcome, but the particular arrangement was plagued once again with nonlinearity at the joint angles. In fact, the rotation of the links relied on the stretching of small tensile springs connected at the ends of the cables. This type of transmission could not possibly yield accurate positioning. Its advantage however lay on the relative simplicity of its design.

As mentioned earlier, a fundamental principle in the design of the new Robotuna was to maximize the accuracy of the joint angles. It was thus clear that a more elaborate compound pulley system had to be developed. Quite naturally, the initial design efforts towards this issue attempted to produce a perfectly coupled compound pulley system that would adopt the design philosophy of the later joints. Unfortunately, it was impossible to incorporate the two together in a robust and reliable design. As a result, the opposite extreme was investigated. It was found indeed that the joints could be perfectly decoupled by positioning one end of the compound system at the center of the preceding bulkhead and by allowing the other end to translate freely in a diagonal direction. Attached to the second end was a short stainless-steel cable that connected it to the next bulkhead. The latter was rounded by means of removable aluminum ears to provide a linear angular relationship. Figure 2-9 is a closeup view of the compound-pulley system of joint 1 and shows the general arrangement.

This type of arrangement guaranteed perfect decoupling. By concentrating the two compound pulleys to the center of the previous joint, the overall system was oriented in a purely radial direction from the joint. Conceptually, the effect of this action would be similar to the effect of a pair of conduit idler pulleys with a vanishingly small radius, as shown in Figure 2-10 and Figure 2-11.

A small amount of partial coupling was admitted only to the system controlling the first joint (joint 0). This "relaxation" in the design had to be made due to the lack of available space. More specifically, the positioning of the cable distribution system (mainly composed of tightly spaced fiddle pulleys) resulted in a small conflict with the compound pulley system and required the rerouting of a cable. This procedure slightly
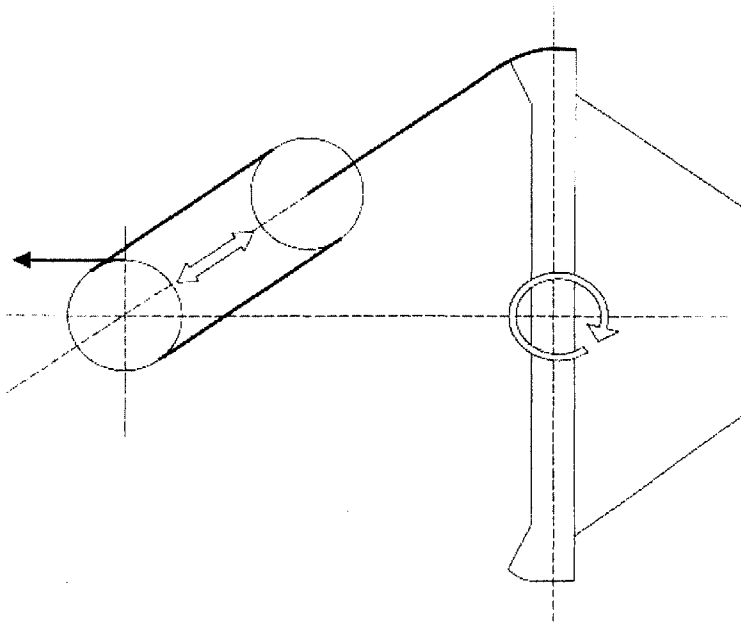
Figure 2-10: Schematic diagram of Compound Pulley System. The pulley at the left is fixed while the one diagonally to the right is allowed to slide, thus rotating the bulkhead that is attached to.
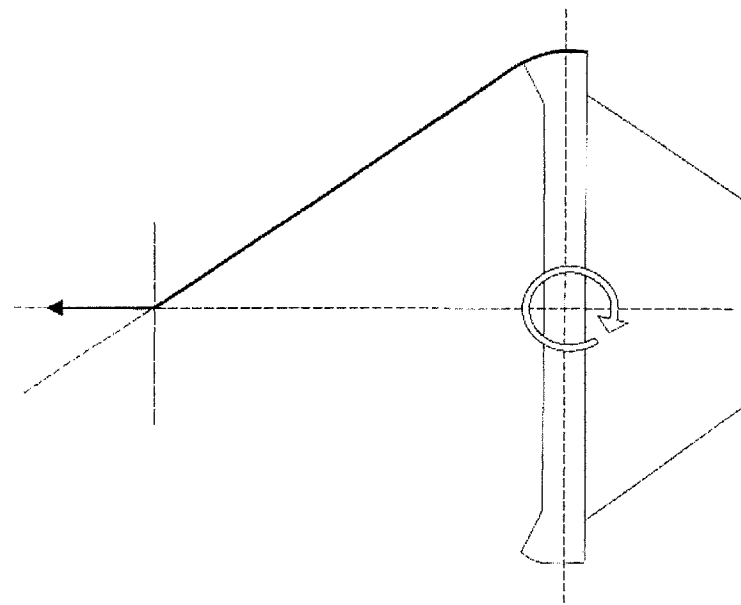
Figure 2-11: Abstraction of the Compound Pulley system of Figure 2-10, showing the similarity to a perfectly decoupled transmission system.

compromised coupling and also introduced a small nonlinearity. Future designs should be wary of this problem and could attempt to resolve it.

From a design point of view, the proposed compound pulley mechanism was a risky solution to the problem of transmission, since it allowed for two pairs of freely translating pulleys (one pair for clockwise and one for anti-clockwise rotation). To secure the proper translation of these pulleys, it was decided that they should mounted on linear guides of stainless steel, that slid in appropriately shaped channels of delrin. Vibrational stability, proper alignment and wear constituted the main concerns of this decision. The results were quite satisfactory and eliminated the initial fears. Had it not been for space limitations and for friction considerations, one could even consider adopting this decoupled compound pulley system as the main principle behind the entire transmission design.

2.2.3 Reflections to the Transmission System Design

The transmission mechanism of the new Robotuna as described above can be classified as a hybrid case. Even though it was based on cable-drive principles, it was flexible enough to incorporate a fundamentally different philosophy of a bar-linkage drive. Furthermore, the question of joint coupling in the links seems to be more involved: joints 0 and 1 are fully decoupled, joints 2 and 3 are fully coupled and joint 4 is partially coupled in a very specific way. At first, it may appear that all these optimization decisions have merely resulted in complicating the transmission system of the fish and have thus made the task of controlling the Robotuna unnecessarily dreadful. In fact, the opposite is true. The motion commands are almost perfectly linearly connected to the position outputs and, as a result, can be computed in a very straightforward manner. Moreover, there is significantly higher confidence over the actual position of the links without the use of position sensors, which reduces the need for active position tracking.

31
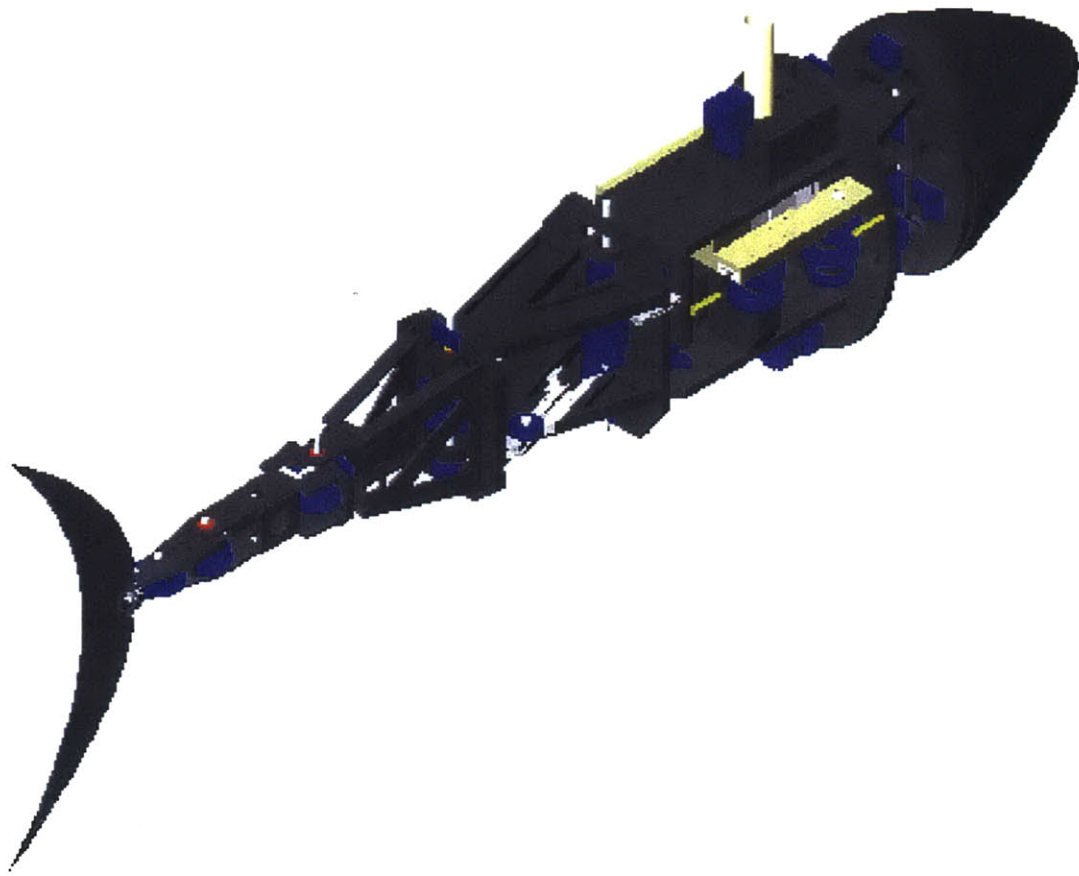
Figure 2-12: Overview of the final assembly of the new Robotuna, as designed in SolidWorks by D. Beal and the author.

2.3 Position Sensor Considerations

During the early stages of the design of the new Robotuna, it was considered prudent to allow for the possibility of active feedback position tracking on the joints. The importance of accurate positioning was stressed in a previous section and cannot be overemphasized. Thus, even though the new transmission mechanism is designed to reduce the need for a tracking system, the latter may appear to be increasingly valuable as the Robotuna ages. Indeed, corrosion effects, replacement of vital parts with slightly different ones, as well as possible changes in the skeleton in the long term could introduce uncertainty that would have to be eliminated only with feedback.

In the old Robotuna, position sensing was a task left entirely to the angular position encoders that were mounted directly on the driving motors. The major benefit of this type of measurement is the overall simplicity of installation. Safely above the water surface, the encoders can give accurate measurements of the commanded positions of the rotors. Unfortunately, this is not sufficient to describe the actual joint angles, mostly due to complications arising from the dynamics of the compliant steel cables. A model can be constructed to account for these undesirable effects, but a more straightforward solution is sought instead which bypasses the cable dynamics and allows for collocated sensing on the joints.

The choice of the sensors was based on three necessary criteria: the sensors should be within one degree accurate, fully water-tight and sufficiently small to fit in a very constricted geometry. Microminiature DVRT type sensors were selected as the most desirable candidate. These are highly sensitive, state of the art linear displacement sensors that detect the differential change in reluctance caused by the motion of a miniature permeable core within two coil windings. They are about 1 inch long, water-tight, and have the ability to screen out thermal effects. Moreover, they have been used successfully in the hydraulically actuated Robotic Tuna that was built in Draper Laboratories.

Even though these sensors are linear, they were chosen over angular displacement measuring devices due to their exceptionally high sensitivity and reliability. This,

POSITION DIAGRAM FOR SUPPORT LINKS OF DVRT 4

Legend:
- fixed distance on bulkhead
- DVRT
- fixed distance perpendicular to DVRT
- fixed distance
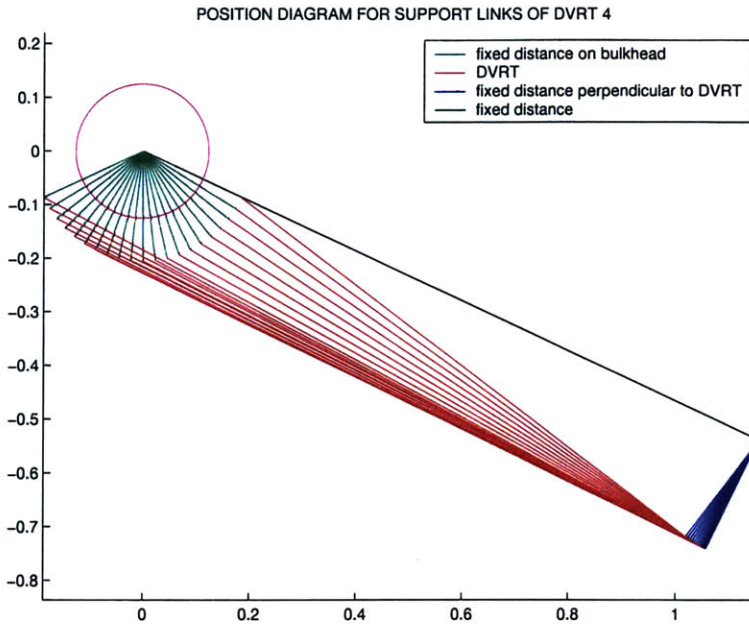
Figure 2-13: Schematic of the DVRT set up as it changes position with different angles. The purple circle designates the size of the bearing mounted on the relevant joint. The green segment describes a fixed distance from the center of the joint to the attached bulkhead. The DVRT is mounted on the red line (of variable length). The black and blue lines are legs of constant length, fixed or pinned to the rest of the mechanism.

of course, required that their mounting mechanism had to be designed carefully to convert linear to angular displacement. Naturally, one would desire a very simple and compact scheme that would be as linear as possible and that would not introduce any position error. Unexpectedly, this developed to an intricate optimization problem, where angular range, spatial constrains, sensitivity, linearity and monotonicity in the relation between linear and angular displacements, often played conflicting roles. As a consequence, the set up for each joint's sensor had to be different, to reflect the characteristics of the particular joint. In all cases however, the conversion from angular motion (of the joint) to the linear DVRT motion was achieved by means of a four-legged linkage system. Geometrically, this corresponded to a four sided structure with one variable angle and one variable length, as shown schematically in Figure 2-13. The installation of one of the DVRTs on the Robotuna is shown in Figure 2-15.

NONLINEAR MAP FROM LINEAR TO ANGULAR DISPLACEMENTS
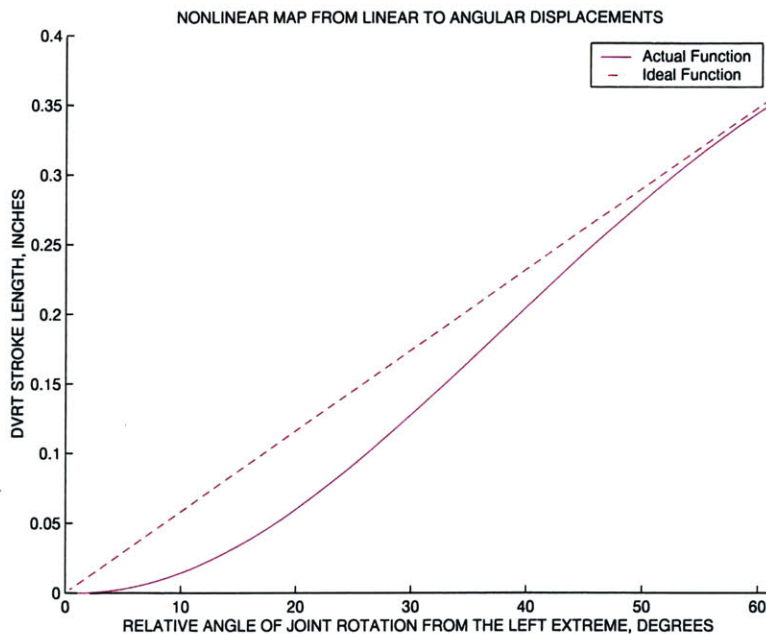
Figure 2-14: The purple line shows the functional relation between DVRT core displacement and joint rotation for joint 4. Extreme angle positions at 0 and 60 degrees (straight fish at 30 degrees). Monotonicity is preserved but not linearity, as the deviation from the ideal red line shows. Sensitivity is also expected to be lost near the lower extreme.

Clearly, this was an inherently nonlinear model, but the parameters of the mechanism were chosen in such a way that the effect of the nonlinearity was reduced so that it was apparent only at extreme angles, close to or beyond the limits of the joint's allowable angular range. This effect is shown in Figure 2-14 for the DVRT of joint 4.

The position measuring system just described was the simplest solution to the problem of accurate sensing of the joint angles. So far though, in its four-month life, the Robotuna has operated without these sensors. This decision was made partly to simplify the task of preliminary testing and also to establish that the operation of the tuna was smooth and a typical swim would not be likely to threaten the extremely delicate and expensive DVRTs.

Finally, it can be stated with certain confidence that the ability to produce enough thrust for self propulsion is a good indicator that the compounded error of the joint

35
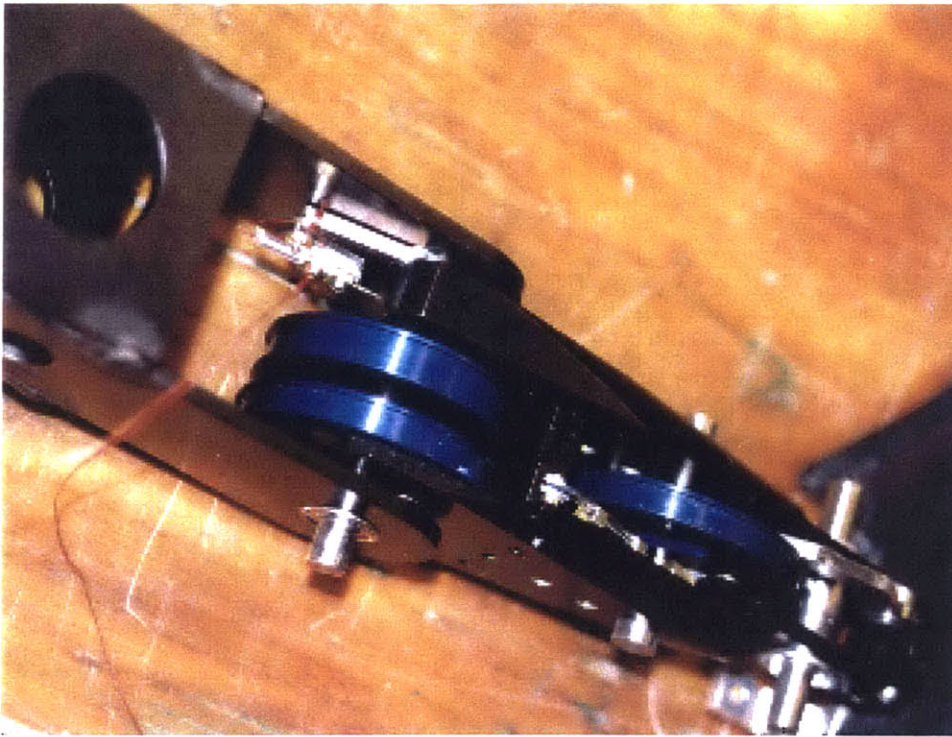
Figure 2-15: Closeup view of the DVRT placement for joint 4.

angles is sufficiently small for the preliminary tests that have been conducted, and therefore position sensors are not yet critical for operation.

2.4 External Shape Design Considerations

2.4.1 Relevance of the Problem

To perform a detailed study of the dynamics of fish swimming, it is essential that the Robotuna must resemble an actual fish as closely as possible. This suggests that apart from the obvious need for a smooth, periodic undulation, it is important to replicate accurately the external characteristics of its shape. The metallic skeleton structure is not an acceptable imitation of a tuna's body. In fact, it is hardly any different from a typical, five-link robotic arm and resembles a fish form only in the most stylistically abstract way. The task of camouphlaging this mechanical assembly of links and pulleys to a convincing bluefin tuna form is precisely the main concern

behind the rib and skin design. The weight of this design task was undertaken by senior undergraduate student, Michael Jakuba[7]. For this reason, I limit myself to an outline of the main concerns of the design and a brief description of the solutions that were adopted.

2.4.2 Design Concerns over the Skin and Ribs

Barrett's solution to the issue of a smooth thunniform shape provided for a thick layer of skin that lay over a system of ribs and foam. The skin was a composite of lycra, latex and foam layers. The lycra served to reduce small irregularities in the foam and was used as the outer layer. The purpose of the foam was to average larger irregularities and to eliminate any bumps caused by the ribs during the flexing of the body, an effect frequently described as the "hungry dog" look. Finally, the latex sheets strengthened the stiffness of the skin and assured that it was tightly wrapped around the body at all times. Underneath this complex skin there was a section of thick "flesh" and "bones", trimmed appropriately to resemble the shape of a tuna. The "flesh" was composed of highly porous foam segments, separated transversely by plastic ribs that were fixed on a common spine. This system conveniently filled the space between the metallic skeleton and the composite skin, and served two important functions. Firstly, it generated the general shape of the tuna by allowing the skin to contact it. Secondly, it provided an energy storage mechanism, by compressing like a spring at large joint angles and then releasing this elastic potential in the form of useful kinetic energy, thus reducing the required peak amplitude of the input power of the motors.

On the negative side, this type of massive flesh reduced the amount of available space within the fish's body. Furthermore, it caused some difficulties near the tail section, where the cross-sectional area of the outer hull was only slightly larger than the enclosed peduncle, leaving little space for flesh and skin. Moreover, it reversed the advantage of energy storage by inducing major power losses. These losses were primarily due to a cyclic pumping effect of the entrained fluid, caused by the contraction and release of the foam. As the fish aged, the elastic properties of the foam

deteriorated and its structural damping increased, thus leading to even higher levels of power losses. Finally, another disadvantage of this particular flesh design was the difficulty and time involved in its installation and removal, which were necessary in order to expose the skeleton. This is often necessary for inspection and maintenance reasons. As a consequence, it was highly desired to construct a rib and skin design that was more readily removable and did not require hours spent on removing and re-attaching each and every rib and foam segment.

2.4.3 Design Solutions on Skin and Ribs

The design scheme of the new Robotuna was fundamentally different from what was described above. Instead of large, disc-shaped rib structures surrounded by foam, a peripheral rib cage was used, very similar to the one used in Kumph's Robopike [8]. More specifically, the ribs took the form of thin, metallic rings, spaced closely together and connected axially by means of two flexible splines that are pivoted to the joints in a way that guarantees smoothness in the swimming profile. A side view of this assembly is shown in Figure 2-16. These rings define the desired thunniform shape and provide a rigid surface where the outer skin can attach, far away from the robotic skeleton. The issue of flesh is avoided completely, resulting in a very light overall structure that does not interfere significantly with the mechanical links of the core and that conveniently leaves plenty of "empty space" to be occupied by pressure sensor gear. A more detailed description of this will follow in a later chapter.

More importantly, this peripheral cage-like rib structure can be removed and re-installed with minimal effort, almost like a sock. It also allows for the possibility of installing alternative fish shapes to the same skeleton, if so desired in the future. To avoid a hungry dog look, the ribs are coated with a thick layer of overlapping scales. These scales bear little resemblance to what is found in actual fish, but have been designed to play a similar role. They are composed of very thin, 3inch-by-1/2inch pieces of vinyl and have been pinned permanently to the outer surface of the ribs. As they overlap each other, they create a very smooth surface that can be easily stretched and contracted and that allows for low water permeability. It is indeed a very elegant

38
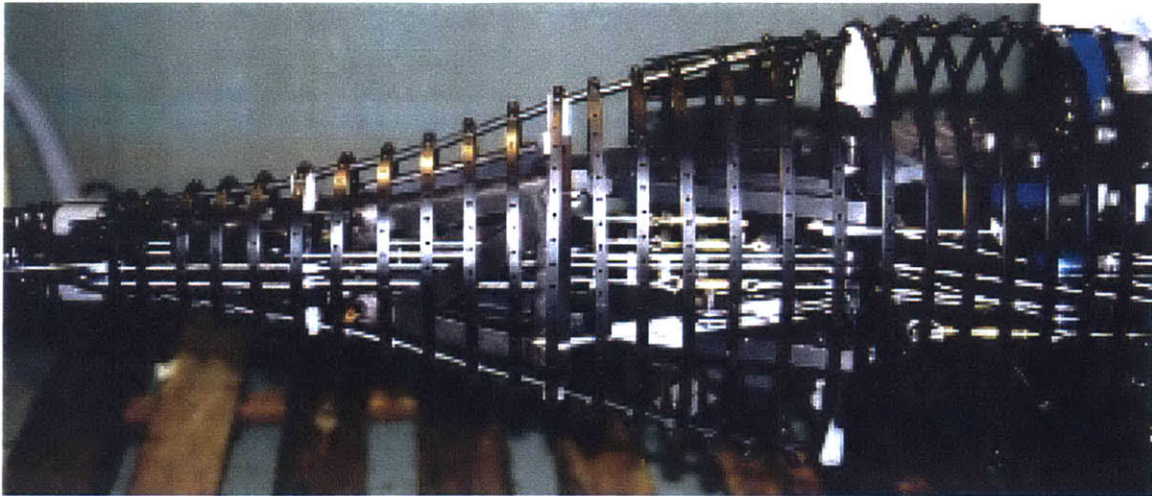
Figure 2-16: General view of the spine and rib design.

solution to the issue of external smoothness, developed by Jakuba. Finally, despite the fact that the pinning of the scales on the rib surfaces was a very time intensive exercise (there are more than 1000 scales currently pinned on the outer structure of the tuna hull) it was a very desirable technique in the long run, since the pinning was meant to be permanent.

Exterior to the scales lay the outer skin in a way that resembles the skin/scale formation in real tunas. Unlike Barrett's composite skin, the new one involved only a thin layer of lycra. The addition of a foam layer was deemed unnecessary, since the hungry dog look was sufficiently reduced by the scales underneath. Also, the latex stiffening layer was eliminated as it was impractical: latex has been found to lose some of its elastic properties with time, when exposed to highly chlorinated water, and can easily tear catastrophically. Moreover, the omission of foam reduced its importance, as there was no special concern over tightness.

As was proven very early on, this thin and light outer skin structure resting on a mesh of overlapping scales resulted in an exceptionally smooth external fish profile, very suitable for laser based visualization techniques, such as DPIV.

A sole notable disadvantage of the scale structure is that it introduces significant power losses, mainly as Coulomb and linear friction between the individual scales. From a design point of view, one only has to consider that the new tuna has more

than a thousand moving parts, each making its own contribution to the overall losses. The power losses to the skin have been measured to be of the order of 30% of the total frictional losses of the mechanism. This, of course, is an issue of significant concern, but steps have been taken to cancel out the effect. An analytical description will follow in the next chapter. Nevertheless, it is worthy to remark at this point that the largest contribution of the scale losses does not come from scale-to-scale interactions as might have been expected, but from the contact between scales and the thin silicone elastic bands that are used to keep them in an orderly manner[7]. A better choice for these bands could perhaps make a marked difference in the power consumption.

2.4.4 Nosecone Design

The design of the front section of the fish was also an issue of some concern. In compliance with the old Robotuna, a rigid nosecone shell, 8 inches in length, was attached to the first bulkhead of the mechanism. As described earlier, this bulkhead has the capability of performing an anticlastic motion defined by the first joint (joint 0).

The shape of the nosecone shell was measured in vertical segments from the cast of a real bluefin tuna. To a good approximation, it can be described as a collection of elliptical cross-sections, with varying eccentricities. Having determined the shape, a wooden model was developed and then used to thermophorm a 1/8" PVC layer. Figure 2-17 shows the actual wooden model with a thermoformed layer. For reasons of external rigidity, the shell was subsequently re-enforced with an inner elliptical bulkhead of aluminum, as well as with a thin layer of epoxy.

A major improvement over the nosecone of the old Robotuna and a subject of particular emphasis was the transition from the rigid cone to the first bulkhead and the flexible rib structure behind it. This occurs only 8" away from the tip of the fish. Evidently, the Reynolds number at that location is not fully turbulent for all possible operating speeds. Consequently, if the transition is characterized by large gaps or extrusions, it is possible for the flow to separate, especially since turbulence
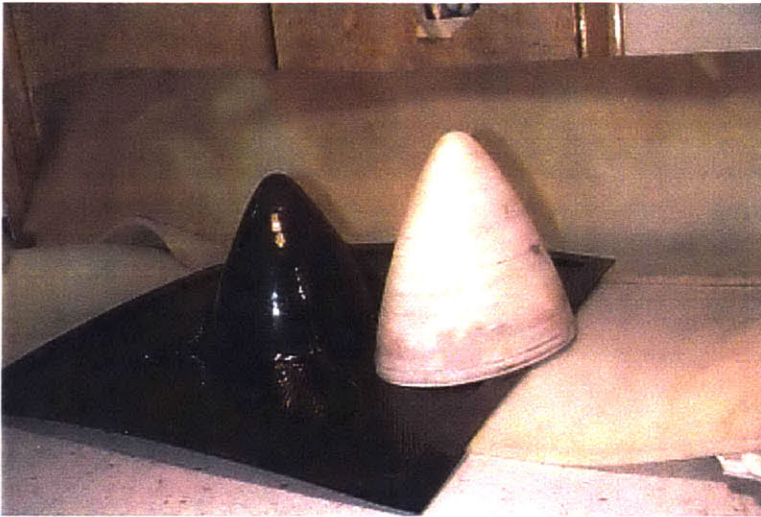
Figure 2-17: Wooden nose model and actual nosecone, thermoformed from a square PVC sheet

may not be present to stabilize the boundary layer. Such a disturbance in the flow may contribute significantly to the total drag and, more importantly, may disrupt any possible vorticity control mechanism employed by the tuna for efficient propulsion. In fact, the nosecone transition was so poor in the old Robotuna, that a silicon collar had to be placed as an easy, but temporary and inelegant, solution[16].

The Robotuna design solved the transition problem permanently and elegantly in three ways. First of all, it provided for two pairs of mounting blocks that were attached to the inner part of the first bulkhead and served as anchors for four plastic tubular springs residing inside the nosecone. This design solution was offered by David Beal and avoided completely the need for external connections. The spring-loaded cone was then capable of maintaining a fixed position with respect to the bulkhead during swimming. Secondly, a ring of scales was attached to the end of the nosecone, thus making the rest of the body a natural extension of the cone[7]. Finally, the nosecone was allowed to be covered completely by the thin lycra skin, thus creating a very uniform outer surface throughout the entire body of the Robotuna.

2.4.5 Peduncle and Tail Regions

The peduncular region offered yet another challenging design issue. As mentioned in the section on Actuation, this region hosts the peculiar lateral keel, which in the case of the Robotuna had the form of a disproportionately large driving pulley centered along the mid-height of the fish, just a few inches before the tail section. Clearly, the ring-like structure of ribs that was described previously could not possibly produce such an odd geometry, whose characteristic radius of curvature was also much smaller than the length of the scales. A clever solution was produced by Jakuba and called for a specially molded shell of rubber-like cast that could easily be inserted or removed[7].

A few inches back, the tail fin was clamped to axis 5 of the robotic arm. This was done very similarly to Barrett's approach[1]. The tail used was a lunate polyurethane cast, based on actual tail dimensions. Though mostly inflexible and especially in the spanwise direction, it allowed for some slight lateral deformation near the tips.

2.4.6 Fins and Finlets

Following the tradition of the old Robotuna, two fins were installed, a dorsal and a ventral. These are inflexible and unretractable, and are fixed rigidly on the upper and lower splines.

In the early stages of the new Robotuna design, it was considered necessary to model the dorsal and ventral arrays of triangular finlets of the peduncle region. The position of these finlets near the tail suggests that they might actually contribute to the propulsion mechanism of the fish. Potential theories for their use are abundant, but it remains largely unclear what their function is. According to some, the finlets help to reduce three-dimensional flow effects and direct the flow to the tail where the vorticity can be properly utilized for efficient propulsion. According to Lauder who has studied finlets of thunniforms, this is not a very likely scenario[9]. Even if there is some active control on the finlets, they are too flexible to have a significant effect on the flow. Indeed, it would be very surprising if they contributed to the overall efficiency by more than 1%. For this reason, the idea of building such finlet arrays

and installing them just prior to the lateral keel section, was considered to be an unnecessary complication of unlikely benefit, and thus abandoned.

2.5   Evaluation of the Robotuna's Design

The new Robotuna has been swimming in the MIT Towing Tank since the beginning of February 2000. During its four-month operation, many swimming styles have been performed and studied. An analytical description and interpretation of the results that have been obtained so far are the main subjects of the next chapter. Nevertheless, it is worthy to make an early evaluation of the tuna's performance and relate the conclusions to some of the design decisions described earlier.

First of all, it is important to note that throughout its life, the new Robotuna has not experienced any mechanical failures. This is largely to the credit of David Beal, whose operating software programming is capable of setting limits on the motion parameters, detecting unstable outputs early on and aborting dangerous swimming styles before catastrophe occurs. Furthermore, this is an indication that the overall design of the skeleton has met successfully the parameter range specifications that were imposed. In fact, very few swimming styles led to instability and had to be aborted. Usually, these corresponded to awkward combinations of motion parameters that were not expected to produce "healthy-looking" fish. More careful fine tuning of the motor gains could have restored stability for these runs, but this was not considered an important task to pursue.

Another characteristic feature of the Robotuna's performance was that it is capable of producing enough thrust to propel itself at a nominal cruising speed of 0.6 m/s. This was of the order of 2N, or the equivalent of a weight of 200g. At times, the total thrust was even twice as what would be necessary for self propulsion. This suggests that the joints are capable of outputting high levels of torque and thus of doing work against the surrounding fluid without being swept by it, as was the case in the last stages of the old Robotuna. This obviously marks a victory for the overall design of the transmission mechanism. As expected, the cases of high thrust production were

associated with high Strouhal numbers, which occasionally approached 0.4 (based on the double amplitude of the tail's heave). Even at such vigorous undulations of the body, the fish was able to maintain a smooth swimming profile, free of kinks or other discontinuities that might disrupt the flow. It is therefore fair to claim that the outer hull design of the skin, ribs and scales was a notable success in this respect.

Finally, it should be remarked that the average power consumption of the motors was nearly as high as the Old Robotuna's. Typical figures of total power loss ranged from 1 Watt to 5 Watts. This marks a very high level, considering that approximately only 1 Watt is required to tow the fish at the operating speed of 0.6m/s. Also, as much as 30% of this power consumption originates from the outer hull. The rest is primarily lost to the cable drive mechanism and to the wake behind the fish.

Having outlined these general trends from the preliminary test performance of the Robotuna, it is now time to analyze them in more detail and investigate ways of improvement.
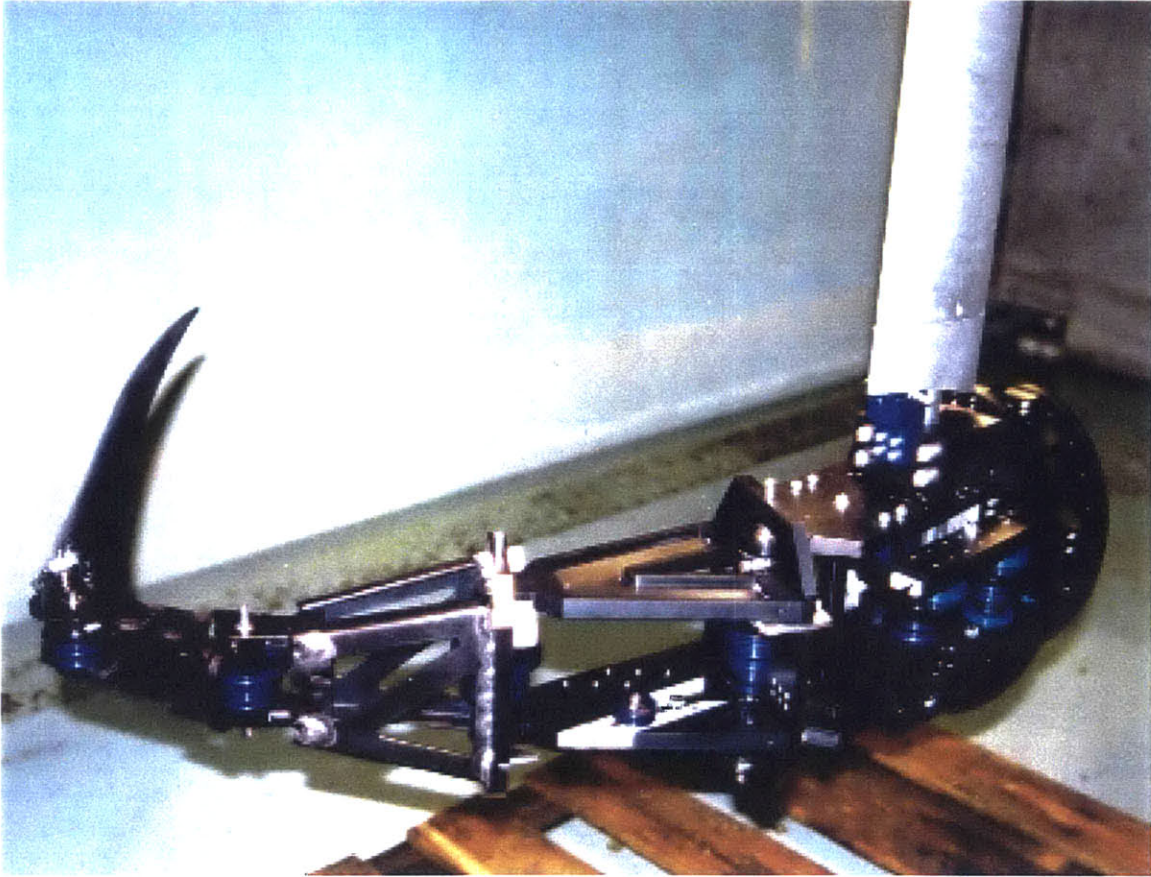
Figure 2-18: The new Robotuna posing at the final stages of its assembly. The cables have not been threaded yet.

Figure 2-19: Another view of the Robotuna, just prior to the installation of the cables.

Chapter 3

Testing and Performance of the New Robotuna

3.1 Preliminary Test Results

The preliminary results discussed in this chapter are associated with the first battery of swimming tests that involved the new Robotuna in February and March 2000. Before stating them and attempting to provide explanations, it is important to clarify the nature of these tests, as well as the primary objectives behind them.

3.1.1 Primary Test Objectives

As expected, the test objectives are very compatible with the main objective behind the Robotuna project: to construct an efficient system of underwater propulsion that imitates the undulating motion of a fast moving fish. As a consequence, it is only natural to try to evaluate a swimming style by the propulsive efficiency that characterizes it, which is simply the ratio of average power output to the average useful power input. The latter is considered to be the sum of the power output (which drives the fish) and the total power which is dispensed in the wake. Unfortunately, neither of the components that define this efficiency ratio can be measured directly, all for different reasons. The output power is simply the product of the nominal speed

46

and the total average thrust:

$$\overline{P_{out}} = \overline{TU}$$

While the speed, U, is simply the commanded velocity that moves the carriage, the thrust measurement is inherently coupled to the hydrodynamic drag of the system which cannot be readily computed. More specifically

$$\overline{T} = \lambda \overline{F} + \overline{D}$$

where F is the net force measured between the tuna and the carriage, λ is a known length ratio that converts the vertical load to a horizontal force in the direction of drag, and D is the actual drag of the tuna. This is an equation with two unknowns and thus insufficient to determine the thrust explicitly. A compromise solution can be employed for this reason, by modifying the equation to compute what was termed by Barrett as estimated thrust:

$$\overline{T} = \overline{F} + \overline{D_{straight}}$$

where $D_{straight}$ is the drag of the fish when towed straight at the speed U. It is hoped that $D_{straight} > D$ for a given nominal velocity, a fact that would indicate drag reduction solely based on the undulation of the body. This inequality could be derived from an apparent propulsive efficiency level that exceeds 100%.

The difficulty in the calculation of the useful power input arises from the inability of the tension sensors[1] to separate the propulsive power from the power losses of the driving mechanism. In mathematical terms,

$$\overline{P_{in}} = \overline{P_p} + \overline{P_l}$$

where the first term on the right side designates the propulsive power required to energize the wake and move the fish, the second term describes the frictional power losses, and their sum represents the average power output delivered by the motors. Since only P_{in} is measurable, it has been used to replace the propulsive power in the efficiency calculation:

$$\eta' = \frac{\overline{P_{out}}}{\overline{P_{in}}} = \frac{\overline{TU}}{\overline{P_{in}}} = \frac{\overline{F + D_{straight}}}{\overline{P_{in}}}$$

47

Since $P_{in} > P_p$ at all times, the above definition of efficiency is clearly conservative. Unfortunately, the magnitude of the power loss term can be estimated to be of the same order or even greater than the output. Substituting the propulsive power by the total input power is therefore a very generous gesture which dooms the efficiency levels to disappointingly low values. Furthermore, it makes it almost impossible to discern drag reduction through an increase in efficiency, since the difference between straight and actual drag can be very easily hidden behind large power loss variations. Nevertheless, in lack of a reliable method to estimate the power losses, the generous efficiency form, η', was used as the main criterion for the evaluation of a swimming style.

Had the Robotuna been autonomous, this efficiency metric would have been a sufficient measure to compare and rank different swimming styles. This is not the case however, since the Robotuna is supported, and often driven, by a powerful overhanging carriage system. Self propulsion is not implicitly assumed but rather takes the notion of a performance value. It is therefore necessary to recognize the significance of this value in the evaluation of swimming styles: a slow fish that is incapable of self propulsion may display record high efficiencies and even suggest drag reduction. This is of little importance however, because it does not reflect the capabilities of an autonomous structure. As a consequence, a nondimensional thrust number (NDT) was invented by Barrett as the ratio of estimated thrust to straight drag:

$$NDT = \frac{\overline{T}}{\overline{D}_{straight}} = \frac{\overline{F}}{\overline{D}_{straight}} + 1$$

Despite a certain degree of arbitrariness in the definition that describes both the estimated thrust and straight drag, a NDT value of unity implies that no force is exerted between the fish and the carriage, and thus reflects real self propulsion conditions. NDT is therefore a good measure of performance and should be maintained close to 1 for self propulsion.

Even though it can be concluded that NDT and η' are the relevant performance parameters, there is no clear relation between them. This is of course due to the fact that they are two completely independent measures. Consequently, the overall

performance criterion, which will often be referred to as the "Swimming Parameter" (SWP) may be stated in general terms as

$$SWP = f(NDT, \eta')$$

and its exact form is allowed to vary at will between experiments. At this point one may wonder why it is essential to describe the performance of a swimming style in terms of one parameter only. The answer lies in the nature of the search algorithm that is used to detect "healthy-looking" and efficient fish. A swimming style is fully defined by specifying seven independent motion parameters which among others include speed, heave amplitude, Strouhal number and wavelength of body wave (see Table 3.3 for a complete list of parameters.) Searching over the complete parameter space obviously requires a large number of runs, which depends on the "grid" of the search. For instance, if only 10 variations are allowed for each parameter, an exhaustive search would require 10 million runs! This clearly calls for a genetic algorithm approach, where swim styles are constantly evaluated and their performance sets a bias for the domain of the remaining investigation. The genetic algorithm code for the tuna was initially written by Barrett and then modified by Beal.

The details of this algorithm will not be explained in this document, but it is crucial to note that under normal conditions, it is expected to converge to an optimal set of parameters, based on a single, arbitrary criterion for optimality. The swimming parameter then is a natural choice for such a criterion!

It is easy to see that the exact functional form of the swimming parameter may favor a certain class of swim styles while rejecting another and thus affect the convergence parameter values. Typically, the bias is decided in a way that favors more strongly fish of high efficiency. Self propulsion is generally easier to achieve and can be sought for in the last stages of the genetic algorithm, after a satisfactory efficiency level has been reached.

Many different swimming parameters have been used in the last four months as will be described in later sections. Their shapes vary considerably but they all share three common characteristics which can be stated mathematically as:

49

$$SWP(NDT, \eta') \quad < \quad SWP(1,1)$$

$$\frac{\partial [SWP(NDT, \eta')]}{\partial (NDT)} \quad \neq 0$$

$$\frac{\partial [SWP(NDT, \eta')]}{\partial \eta'} \quad \neq 0$$

$$\forall NDT < 1, \eta' < 1$$

These guarantee that self-propelled fish of very high efficiencies are the favorites in a genetic algorithm, and thus the likely survivors.

It should be noted that these criteria are not sufficient to observe drag reduction and have to be extended for $\eta' > 1$.

3.1.2 Straight Drag Results

One of the first tasks in the experimental list of the new Robotuna was to tabulate the total drag of the fish when towed straight down the tank at various speeds. As shown in the previous section, the straight drag value is essential for the computation of the swimming parameter. An accurate tabulation is therefore required. Moreover, the functional dependence of $D_{straight}$ on towing velocity may help elucidate the flow conditions around the tuna, which are not perfectly clear, as the tuna operates in a transitional Reynolds number range. A standard quadratic model is assumed

$$D_{straight} = \frac{1}{2} \rho c_D A U^2 + D_{mast}(U^2)$$

and the constant friction coefficient, c_F, is determined.

The last term, D_{mast}, is a quadratic term on the velocity which reflects the drag on the underwater section of the vertical mast strut. It is an undesirable term which unavoidably contributes to the measurement of $D_{straight}$. It can be shown to be fairly significant, especially at the high end of the speed range. This is unfortunately the case since its hydrofoil shape has a fairly pronounced curvature. The flow around it has a Reynolds number that does not exceed 10^5 and thus may be laminar and likely
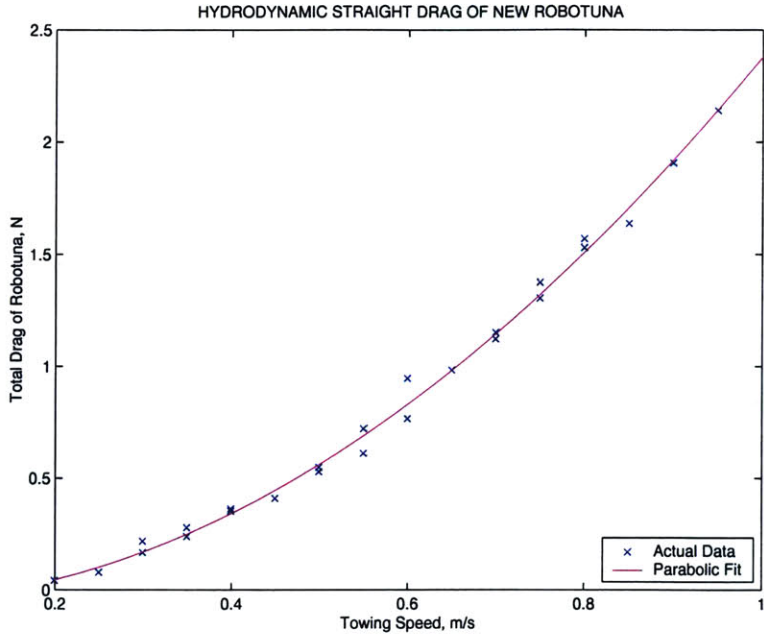
Figure 3-1: First Straight Drag measurements on the new Robotuna and a parabolic fit. These have been very consistent with later measurements during the first four months of operation.
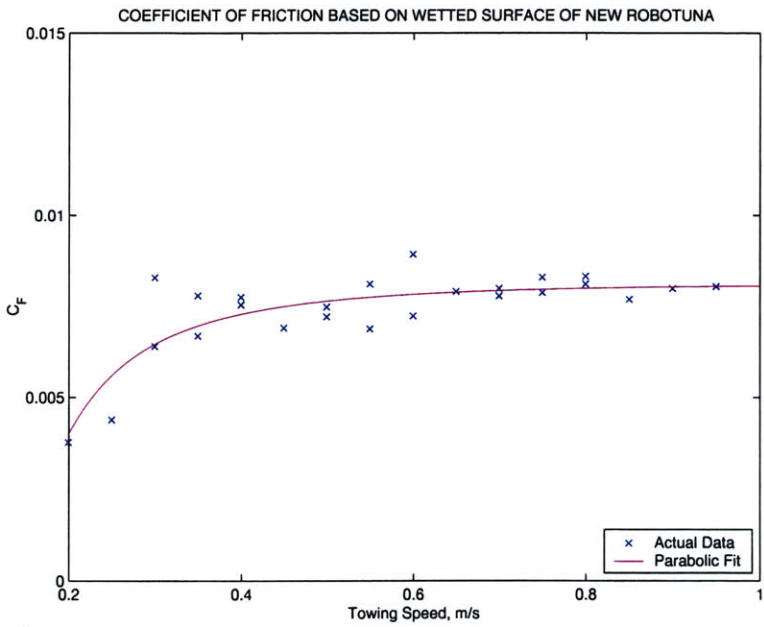
Figure 3-2: Coefficient of friction based on a total wetted area of $0.59m^2$.

to separate early on. Experiments have been performed in past years to tabulate $D_{mast}(U^2)$, by towing the mast only down the tank.

As the plot of U vs. $D_{straight}$ shows in Figure 3-1, the drag may be approximated very well by a quadratic curve throughout the entire speed range (from 0.20 to 0.95m/s). There is no clear indication of transition to turbulence, as that would probably appear as a sudden discontinuous drop in $D_{straight}$. This suggests three possible scenaria:

- The rough Lycra skin stimulates turbulence at Reynolds numbers that correspond to the early transitional region. Thus, c_F is mainly due to turbulent skin friction and perhaps partly due to some late separation.

- Turbulence occurs only near the tail section of the fish. A laminar flow persists, which then separates near joint 0 where the shape curvature is highest. In this case, c_F reflects mostly the form drag of a "bluff body" fish.

- Turbulence occurs only towards the end, and the flow around the fish is laminar. Separation does not occur and c_F mostly reflects the laminar skin friction on the wetted area of the tuna.

The average value of c_F resulting from the curve fit was moderately low, indicating that the second scenario is probably overruled and that separation is not a main concern. Nevertheless, it was quite astonishing to note that the friction coefficient and the drag value at the operative speed of 0.7m/s were almost identical to what was found in the old Robotuna. This was considered to be excessively high in the old Robotuna due to a likely separation induced by a discontinuous transition from the nosecone to the main body. As this problem was thoroughly considered and fixed in the new Robotuna, the drag was expected to be lower.

Possible scenarios to explain this result would attribute some increased drag to the porosity of the lycra skin or to excessive separation from the mast. These suggestions however are not very likely to provide sufficient explanations. In fact, the mast was once covered with a lycra cloth in an effort to trigger turbulence and delay separation. No noticeable effect was observed.

3.1.3 First Genetic Algorithms on the New Robotuna

The results of the first set of genetic algorithms are briefly described in this text mainly for two reasons. The first and most important is that they give a measure of the capabilities of the new Robotuna at the very early stages of its life, when corrosion and wear are in their most minimal states and the tuna is likely to be in its healthiest shape. This means that all measurements should be very reliable and thus facilitate the task of troubleshooting and further investigation. Secondly, these tests are responsible for a critical modification of the efficiency parameter and a new set of experiments that follows. These will be discussed in the next section.

The swimming parameter used in this set of genetic algorithms had the form

$$SWP = (1 + \alpha) \frac{1}{\frac{1}{\eta'} + \frac{\alpha}{NDT}} = (1 + \alpha) \frac{\eta' NDT}{\alpha \eta' + NDT}$$

where α is an arbitrary weight, nominally set to 1. Clearly, the SWP is well behaved at the relevant range of η' and NDT approaches 1 at self propulsion and high efficiency conditions, and has no local maxima for finite η' and NDT. More importantly, for a weight close to the nominal, this SWP favors both parameters equally, so that an optimum swimmer is expected to be capable of both high efficiency and self propulsion. However, since self propulsion conditions are normally easier to converge to, the weight α is sometimes introduced to boost efficiency in the early generations of the genetic algorithm, when the motion parameters have not started to converge. The results obtained with this form of SWP were very consistent between algorithms. For the operating speed of 0.6m/s, the tuna was more than capable of producing enough thrust to propel itself, and at times was even close to doubling it, as Figure 3-4 demonstrates. Unfortunately however, the fish was incapable of producing efficiency levels that exceeded 20%. For the unbiased case ($\alpha = 1$), the evolution curve shifted quickly to the "high thrust" end of the SWP spectrum, favoring only small changes in SWP.

This happened contrary to the desired expectation which was to trace a more rewarding path along $\nabla(SWP)$. The introduction of a strong bias ($\alpha = 0.25$) as an attempt to shift the focus on η' also failed to boost the efficiency. As the penalty

Swimming Parameter with weight 2.50e-001
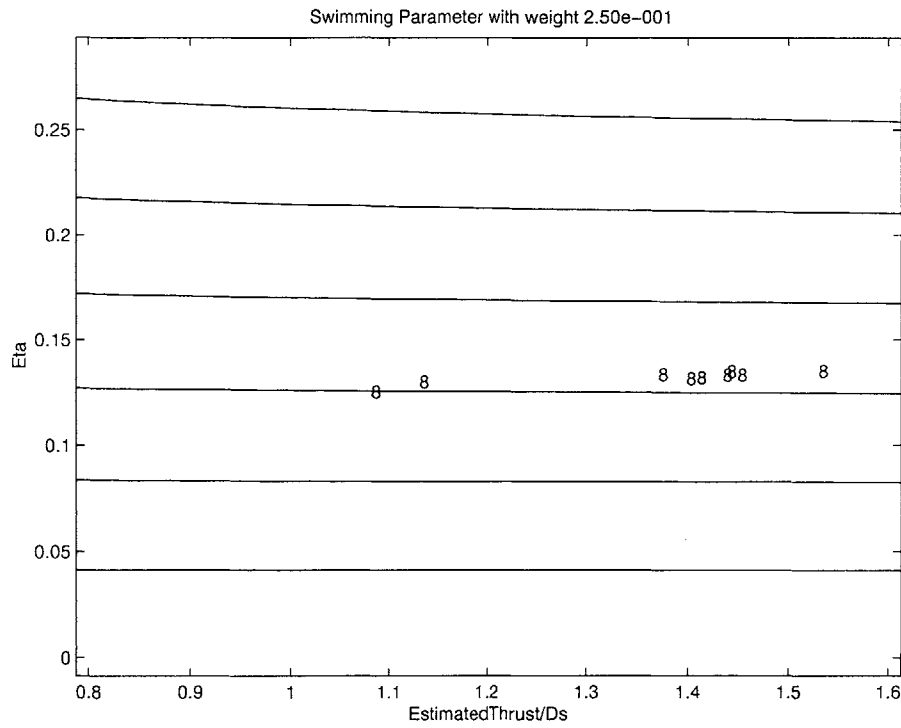
Figure 3-3: Diagram showing the 8_{th} generation of the first genetic algorithm performed on the new Robotuna. As most parameters have reached convergence, it seems that the best swimming style can produce approximately 1.5 times its drag at 0.6m/s, at an efficiency close to 15%. The two low-thrust cases correspond to badly mutated offsprings of the generation.
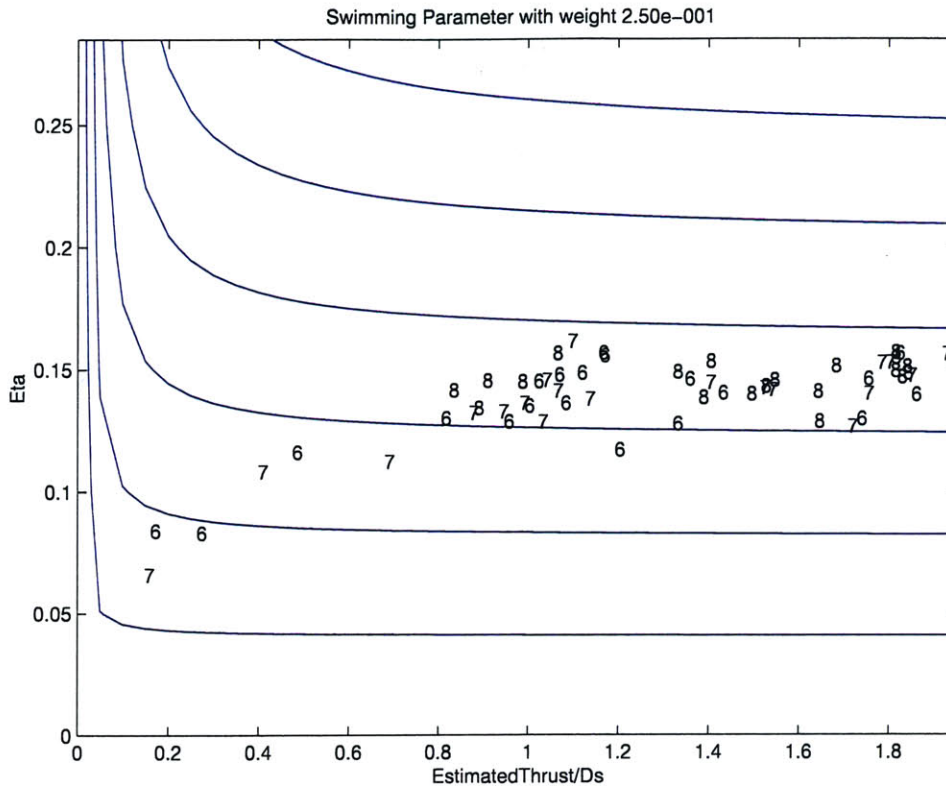
Figure 3-4: Second genetic algorithm performed on the new Robotuna. Only the last three generations are shown. The swimming parameter has a strong weight, $\alpha = 0.25$ and prohibits convergence. Indication of an efficiency barrier near 15% is clear.

of low thrust was removed, late generations failed to converge to a particular set of parameters (and therefore a point in the space of NDT and η'). Instead, they were seen to vary considerably along the domain (NDT, $\eta' < \eta'_{crit}$) where η'_{crit} was a limit barrier to the efficiency level, located near 15% (Figure 3-4).

The message was clear: the maximum efficiency had been reached and was disappointingly low. This led Beal and the author to believe that the low efficiency was partly due to our "generous" definition, which incorporated mechanical losses to the useful input power. For a complex robotic structure, such as the Robotuna that is expected to produce only 1Watt of useful power, the implied condition $P_l \ll P_{out}$ is difficult to satisfy. Consequently, the notable size of P_l establishes an artificial limit to the propulsive efficiency. More importantly, it corrupts the sensitivity of η' to the SWP function, and possibly distorts the converged set of parameters of the genetic

algorithm.

3.2 A Model for the Frictional Losses

As a reaction to the issue of low efficiency, the construction of a model was attempted to predict the power lost to friction. It was soon realized that a full system identification on the Robotuna was bound to be very complex due to the multitude of moving components and the nonlinear interaction with the fluid medium. Luckily, such an approach was not necessary, and a considerably easier alternative was adopted. This was based on the realization that the full nonlinear differential equations for the dynamical system did not have to be solved explicitly in order to derive a model for the average power.

From a Lagrangian standpoint, the Robotuna's dynamics may be expressed as

$$\frac{d}{dt}(\frac{\partial L}{\partial \dot{\theta_i}}) - \frac{\partial L}{\partial \theta_i} + (\tau_l)_i + (\tau_f)_i = T_i$$

where T_i describes the total input torque at joint i, $(\tau_l)_i$ describes the net torque required to overcome frictional losses, and $(\tau_f)_i$ represents the torque contribution to this joint from the surrounding fluid. The total instantaneous power at joint i is then

$$P_i = (P_l)_i + (P_f)_i + \frac{d}{dt}(\frac{\partial L}{\partial \dot{\theta_i}})\dot{\theta_i} - \frac{\partial L}{\partial \theta_i}\dot{\theta_i}$$

from which the time averaged form can be deduced

$$
\begin{aligned}
\overline{P_i} &= \overline{P_{li}} + \overline{P_{fi}} + \frac{1}{T}\int_0^T \frac{d}{dt}(\frac{\partial L}{\partial \dot{\theta_i}})\dot{\theta_i} - \frac{\partial L}{\partial \theta_i}\dot{\theta_i}dt \\
&= \overline{P_{li}} + \overline{P_{fi}} + \frac{1}{T}\int_0^T \frac{d}{dt}(\frac{\partial L}{\partial \dot{\theta_i}}\dot{\theta_i})dt - \frac{1}{T}\int_0^T (\frac{\partial L}{\partial \dot{\theta_i}}\ddot{\theta_i} + \frac{\partial L}{\partial \theta_i}\dot{\theta_i})dt \\
&= \overline{P_{li}} + \overline{P_{fi}} + \frac{1}{T}\int_0^T d(\frac{\partial L}{\partial \dot{\theta_i}}\dot{\theta_i}) - \frac{1}{T}\int_0^T dL \\
&= \overline{P_{li}} + \overline{P_{fi}}
\end{aligned}
$$

This indicates that the measured quantity, which is the net power consumption averaged in time, reflects only contributions from the non-conservative forces that are

present, namely friction and fluidic losses. It is necessary to distinguish between the two because the latter term, $\overline{P_f}$, participates in the computation of the propulsive efficiency.

For this reason, it was decided to swim the tuna in air and thus eliminate the largely unknown $\overline{P_{f_i}}$ term

$$\overline{P_{l_i}} = (\overline{P_i})_{air}$$

The frictional losses were thus directly measurable and a model was constructed to match the measurements.

It should be noted that the possibility that the friction coefficients in the moving parts were different in air than water was considered. The most practical solution to this concern was to frequently submerge the tuna into the water between runs, so as to maintain as wet of an environment as possible. It can be shown however that the power loss marked a slight decrease as the tuna dried up between runs. A typical downward trend is shown in Figure 3-5, where multiple runs have been performed in air at the same swimming style without wetting the tuna. This resulted in a deviation that was well within 5%, and was thus ignored. Moreover, this omission was thought to lead only to slightly more conservative results.

A total of 73 different swim styles were initially tested in air and the power losses of each joint were measured. A model was considered for each joint independently, but more emphasis was given to the first two joints which were responsible for more than 70% of the total power loss. This strikingly non-uniform power loss distribution among the joints did not come as a surprise: they involved a fairly complicated transmission system of translating compound pulleys. At the same time, they were responsible for the motion of a larger number of scales and carried the burden of the nosecone's rotation (joint 0).

The power losses of these joints were modeled in a simple but accurate way, as weighted sums of linear and Coulomb friction components:

$$(\tilde{\tau}_l)_i = \gamma_1 \dot{\theta}_i + \gamma_2 \frac{\dot{\theta}_i}{|\dot{\theta}_i|}$$

57
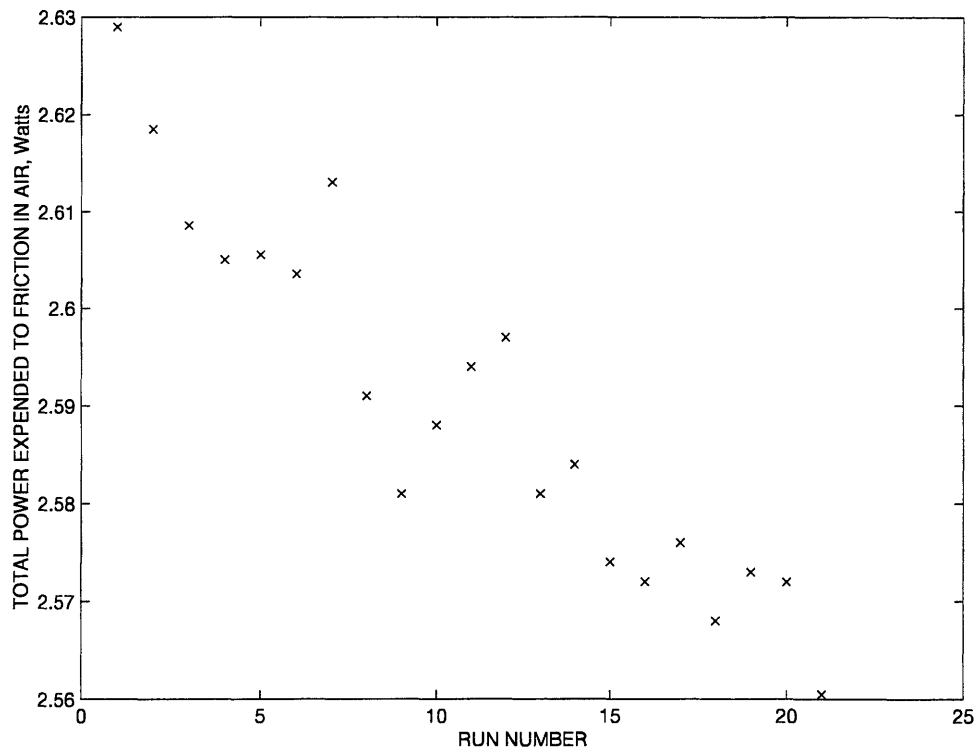
Figure 3-5: Decay in the total power expended to friction in air, as the Robotuna's components become dry. Courtesy of D. Beal.

The power contribution of these is

$$(\tilde{P}_l)_i = \gamma_1 \dot{\theta_i}^2 + \gamma_2 |\dot{\theta_i}|$$

and the time averaged power

$$\overline{\tilde{P}_{li}} = \frac{\gamma_1}{T} \int_0^T \dot{\theta_i}^2 dt + \frac{\gamma_2}{T} \int_0^T |\dot{\theta_i}| dt$$

Since θ_i can be described as a sinusoid of amplitude A_i

$$\theta_i = A_i sin(\omega t + \phi_i)$$

it is trivial to show that

$$\overline{\tilde{P}_{li}} = \frac{1}{2}\gamma_1(A_i\omega)^2 + \frac{2}{\pi}\gamma_2(A_i\omega)$$

The term $A_i\omega$ scales roughly as the Strouhal number for a given operative speed. The power loss at joint i then may simply be considered to be a parabolic function of the Strouhal number only

$$\overline{\tilde{P}_{li}} = \alpha_1 St^2 + \alpha_2 St$$

This result seems to agree very well with the experiments and deviates slightly at high Strouhal numbers.

A least squares fit was performed to determine the values of the constant coefficients. The success of this simple model to predict the power losses of the first two joints in a complicated structure was quite surprising and led to predictions that were well within 10% accurate. This is shown clearly in Table 3.1.

A very similar model was employed to describe the losses at joints 2 and 3 as well. Joint 2 was particularly successful but joint 3 presented deviations that were slightly higher than what would have been expected. As Table 3.1 shows, the mean relative deviations amounted to 10.1% and 25.9% for joints 2 and 3 respectively. It was first considered that the peculiar coupling of the joint to the previous one was the cause of this discrepancy and a new model was constructed to take this into account. The fit turned out for the worse however, so the suggestion was abandoned. It was
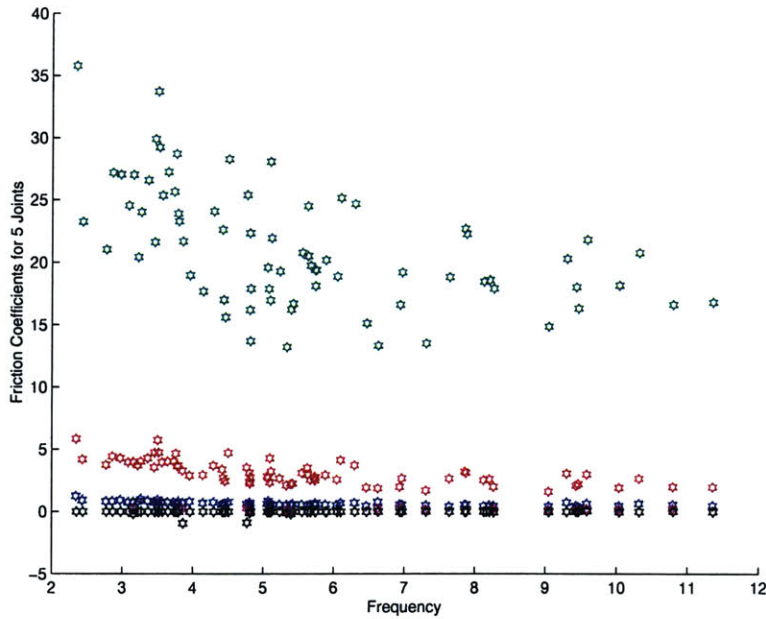
Figure 3-6: Internal friction coëfficients for each joint, calculated from a linear model for friction, as functions of frequency of swimming. Green and red data points correspond to joints 0 and 1 and are the highest. Blue, magenta and black points describe joints 2, 3 and 4. Total of runs: 73
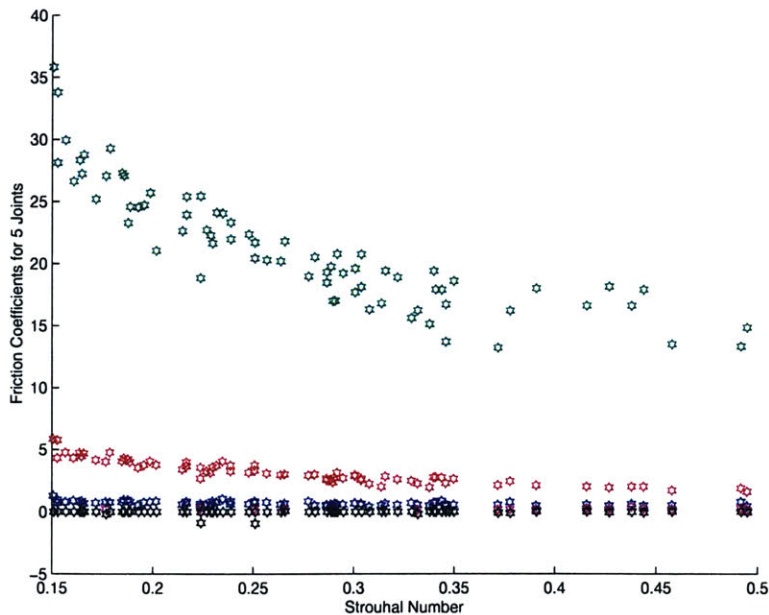
Figure 3-7: Internal friction coefficients for each joint, calculated from a linear model for friction, as functions of Strouhal number. Data seem coherent with a downward slope which suggests the existence of a Coulomb friction component. Total of runs: 73

	JOINT 0	JOINT 1	JOINT 2	JOINT 3	JOINT 4
$\overline{\Delta P}$	0.0711	0.0481	0.0524	0.0731	0.0608
$\sigma(\Delta P)$	0.0691	0.0396	0.0778	0.0901	0.0854
$\overline{\Delta P/\overline{P}}$	0.0710	0.0522	0.1012	0.2588	3.3405
$\sigma(\Delta P/\overline{P})$	0.0523	0.0365	0.1167	0.2323	8.4612

Table 3.1: Mean and standard deviations of actual power expended in the joints from the linear-Coulomb model.

Figure 3-8: Measured (red points) and computed (blue line) power expenditure to friction for joint 0, for a total of 73 runs. The linear-Coulomb model seems within 5% accurate for most runs.

Figure 3-9: Measured (red points) and computed (blue line) power expenditure to friction for joint 1, for a total of 73 runs. As for joint 0, scatter is surprisingly low for such a crude friction model.
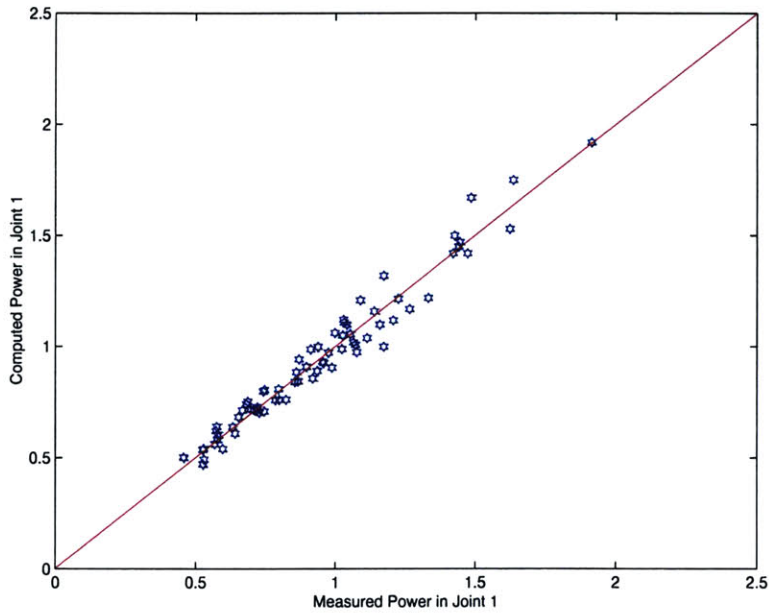
Figure 3-10: Comparison between measured and computed power requirements for joint 1. Agreement is very close for power levels up to 1.1Watt, which describe most swimming styles

Figure 3-11: Measured (red points) and computed (blue line) power expenditure to friction for joint 2, for a total of 73 runs.

Figure 3-12: Measured (red points) and computed (blue line) power expenditure to friction for joint 3, for a total of 73 runs. The accuracy of the model is clearly less than for the first joints.

	γ_0	γ_1	γ_2	γ_3	γ_4
Linear Friction (kgm^2/s)	7.891	0.2348	0.1936	0.0617	0.0161 (not used)
Coulomb Friction (Nm)	2.7914	1.6575	0.2131	0.0505	-0.0412 (not used)

Table 3.2: Linear and Coulomb friction coefficients used to model frictional power losses. The coefficients for joint 4 were not used.

then thought that this discrepancy reflected nonlinear terms. Since the average power consumed in this joint was very small in comparison to the first three joints while the range of the joint angle was higher (and hence $A_i\omega$), it would not come as a surprise to find out that the power loss was more sensitive to higher order terms in $A_i\omega$. The situation in the tail joint (joint 4) was even less predictable as indicated in Table 3.1, so it was decided that a power loss model would not be attempted at all, and that the propulsive efficiency function could afford to be slightly more conservative (by less than 5%) by including this loss in P_{in}. The exact values for the friction coefficients are shown in Table 3.2. It should be emphasized that these coefficients may change in time as the tuna ages.

The total power loss was then described as

$$\overline{\overline{P_l}} = \sum_{i=0}^{3} \overline{\overline{P_{li}}}$$

and a new efficiency form emerged as

$$\eta = \frac{P_{out}}{\overline{\overline{P_{in}}} - \overline{\overline{P_l}}} = \frac{T_e U}{\overline{\overline{P_{in}}} - \overline{\overline{P_l}}}$$

which was expected to be closer to the real propulsive efficiency of the Robotuna.

3.3 Further Genetic Algorithm Results

Equipped with the new metric for the propulsive efficiency, a new genetic algorithm was attempted. The SWP contours were shaped as concentric circles, centered around the desired condition, $\eta_m = 1$,NDT=1, which marked the peak value of SWP=1:
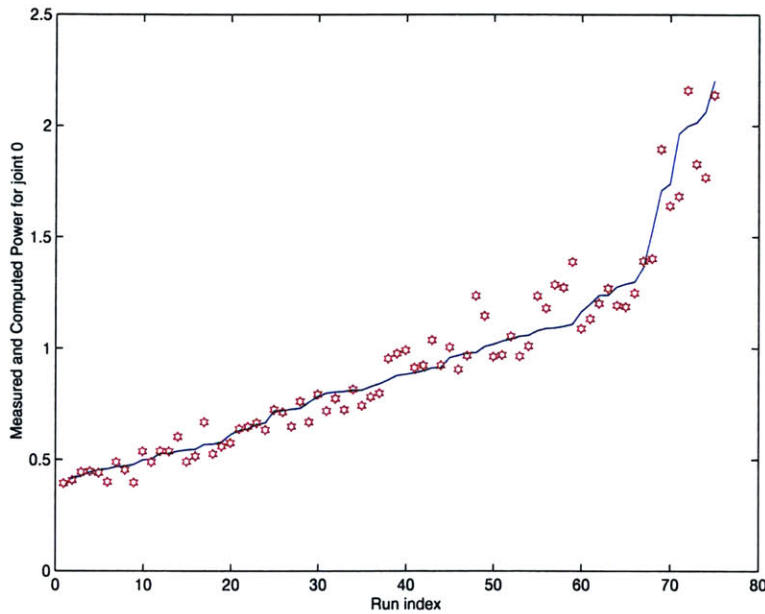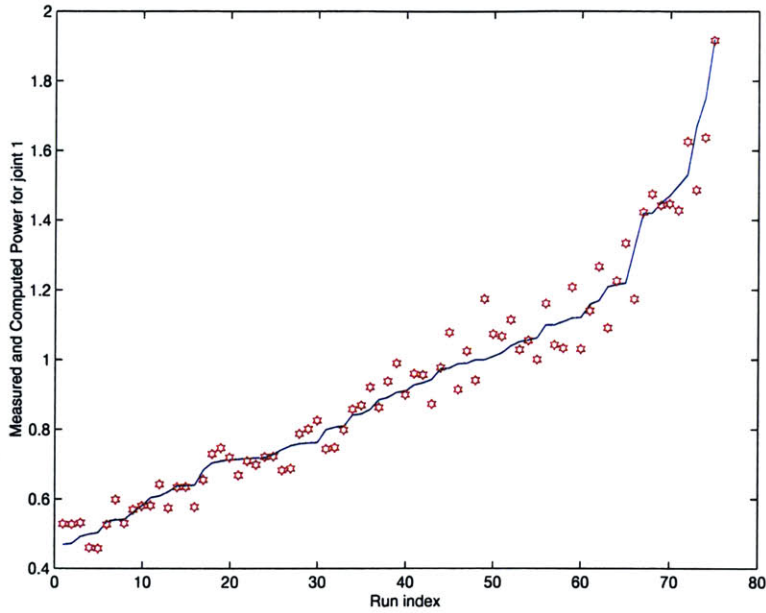
64

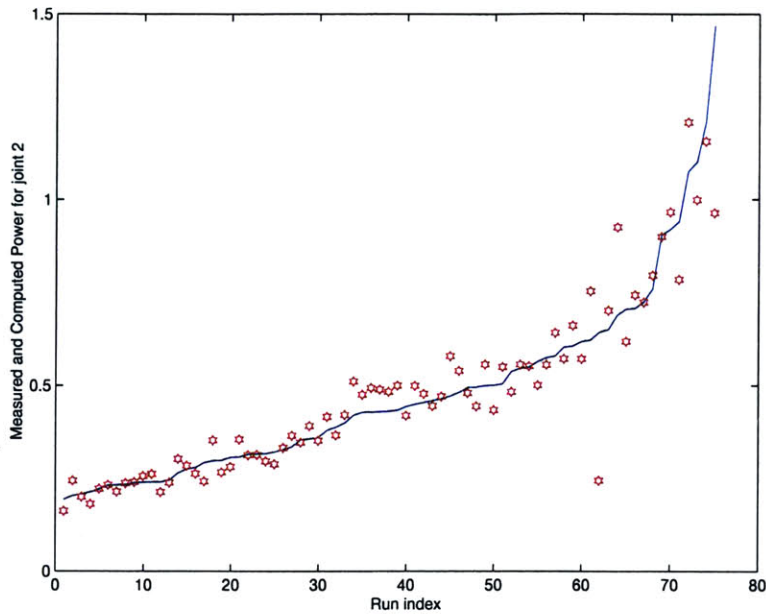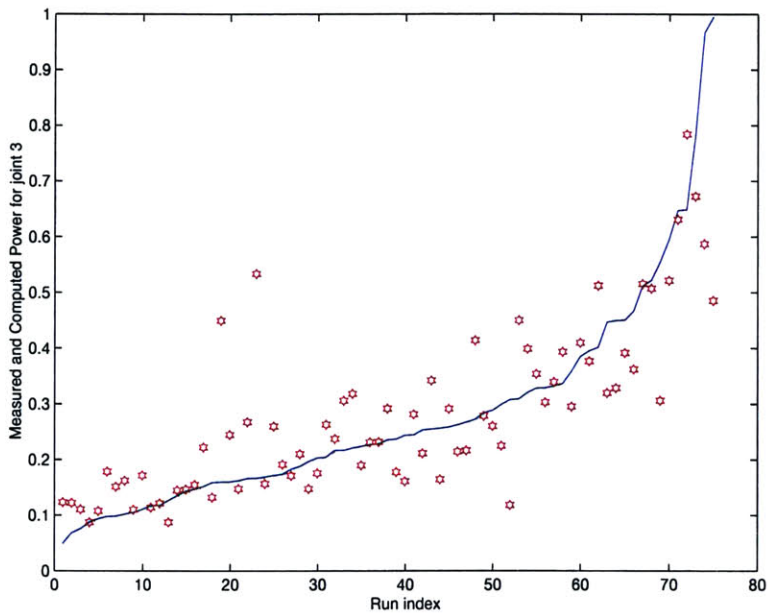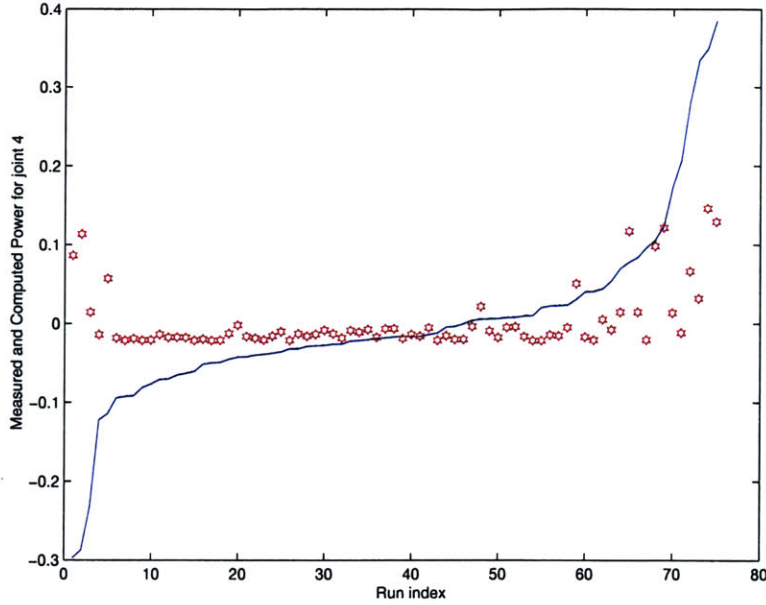Figure 3-13: Measured (red points) and computed (blue line) power expenditure to friction for joint 4, for a total of 73 runs. The model fails completely to follow the data.

$$SWP = 1 - (\eta - 1)^2 - \alpha(NDT - 1)^2$$

The weight, α, was naturally introduced as an optional bias, preserving the topology but offering some eccentricity to the circles.

Figure 3-14 shows the evolution of this genetic algorithm. In general, this choice of SWP seemed to be successful, as evolved swimming styles had the tendency to move towards the optimum center. The extraordinarily high efficiency values in some isolated cases though were taken with some disbelief. These cases were subsequently run in air, to verify the accuracy of the model for the frictional losses. Even though $\overline{\tilde{P}_l}$ was found to be within 10% as expected, the sensitivity of the propulsive efficiency to this uncertainty was unacceptably high, and reduced the real propulsive efficiency to a maximum value of 43% for a fish that was nearly self propelled (NDT=0.95).

For most runs that were vigorous enough to approach the condition of self propulsion, the ratio $\overline{\tilde{P}_l} : \overline{P_{in}}$ was very close to unity. As a result, the uncertainty in efficiency roughly scaled as the inverse of the uncertainty in power losses, producing erroneous conclusions in the genetic algorithm. Had it not been for the penalty that the circular
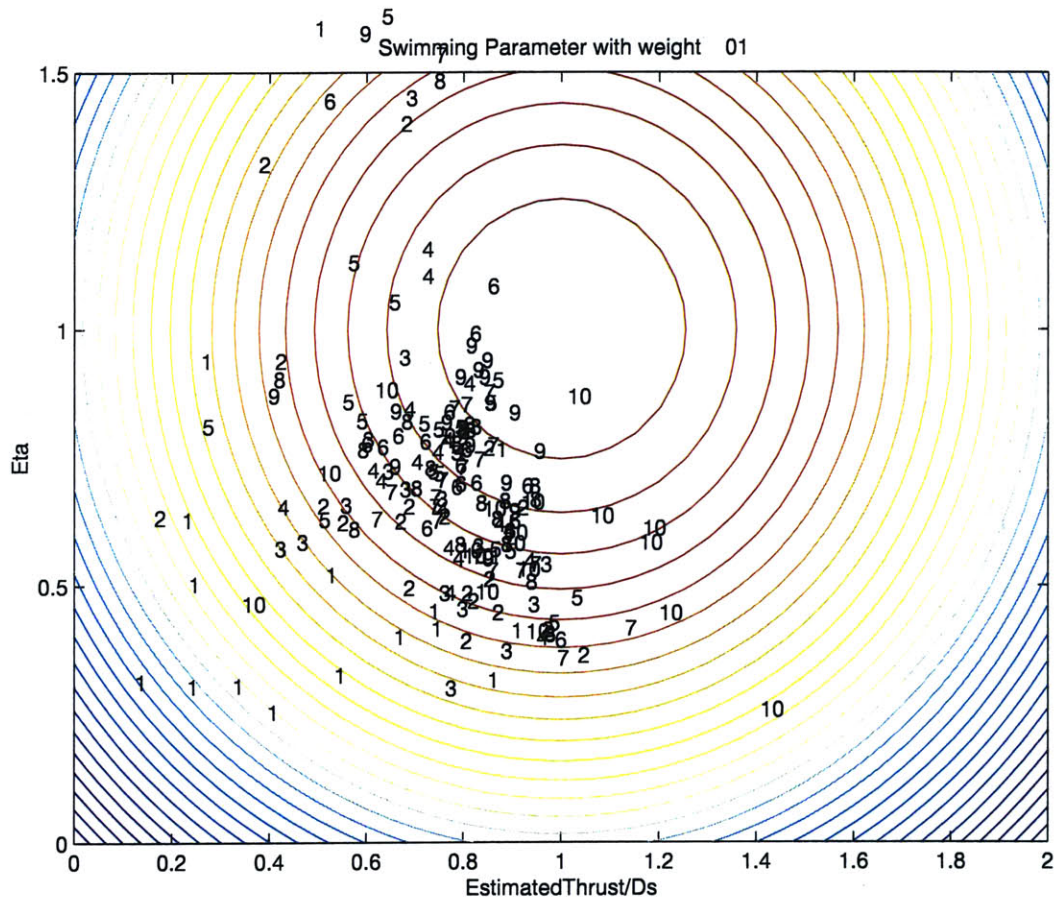
Figure 3-14: Genetic algorithm with circular SWP and a "real" propulsive efficiency that dismissed frictional losses

swimming parameter imposed on efficiency values higher than 100%, the genetic algorithm would have fully exploited this weakness in the power-loss model and would have converged to a suboptimal set of parameters. To restrict this catastrophic effect of model uncertainty, a modified form for the efficiency was developed, which was inherently more robust to it:

$$\eta_m = \frac{\overline{P_{out}} + \overline{\tilde{P_l}}}{\overline{P_{in}}} = \frac{\overline{P_{out}} + \overline{\tilde{P_l}}}{\overline{P_f} + \overline{\tilde{P_l}} + \overline{\Delta P}}$$

where $\overline{\Delta P} = \overline{P_l} - \overline{\tilde{P_l}}$. This modified efficiency is a much more stable parameter to enter the SWP model and participate in the criterion for "best swimming". Furthermore, it possesses two favorable properties. It offers a balance to increased power losses and usually marks only a light increase over the actual propulsive efficiency. The second property may be simply stated mathematically as

$$\eta = \frac{\overline{P_{out}}}{\overline{P_f}} = 1, \overline{\tilde{P_l}} = \overline{P_l} \Rightarrow \eta_m = 1$$

This fact suggests that the previous definitions for the swimming parameter may be employed, simply by switching to the new efficiency measure

$$SWP = f(NDT, \eta_m)$$

After converging to a swimming style that optimizes the swimming parameter, it is a simple task to determine the actual propulsive efficiency by running this particular style in air and determining very accurately the total power loss.

Responding to the ability of the modified efficiency to remain less than 100% for most runs and to the relative ease towards self propulsion, a new genetic algorithm was attempted with yet another swimming parameter. This parameter reflected a somewhat different approach to the issue of convergence: since self propulsion was inevitable, it was decided to allow the algorithm to approach the line NDT=1, and by penalizing higher thrust values, to ascend the efficiency axis. A very simple realization of this thinking was offered in the linear form

$$SWP = \eta_m - \alpha|NDT - 1|$$
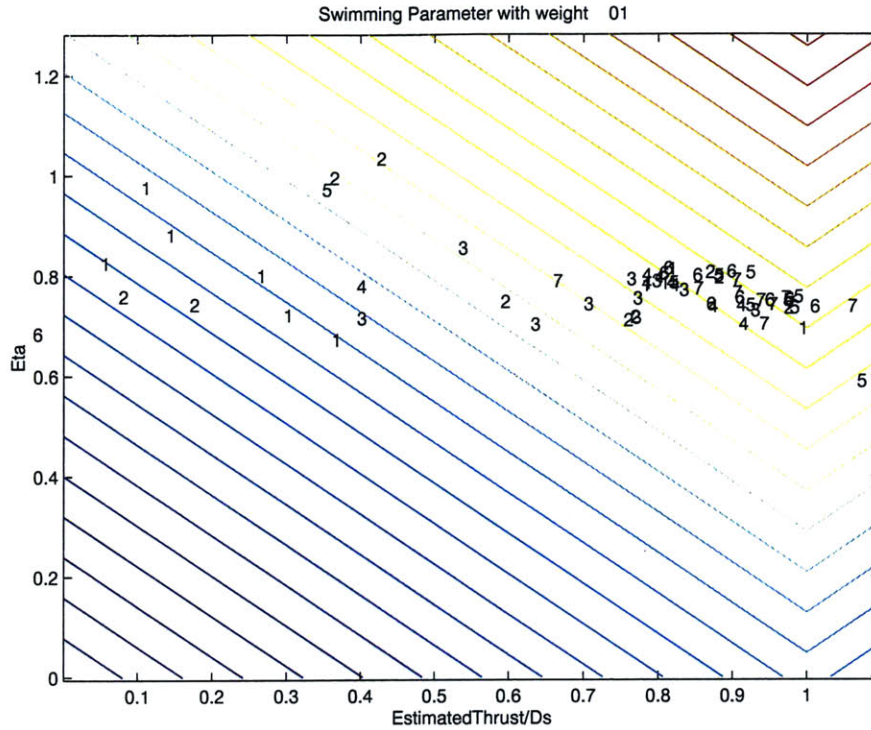
Figure 3-15: Genetic Algorithm with a modified efficiency metric and a linear SWP.

This type of linear function also removed completely any restriction to high efficiency values. The history of evolution of this genetic algorithm is shown in Figure 3-15 and seems to follow closely the intended path. Late generations converged to a modified efficiency of nearly 80%, corresponding to a true propulsive efficiency of 36% at nearly self-propelled conditions. A record efficiency of 49% was produced at an early generation (generation 2) but failed to achieve self-propulsion ($NDT \simeq 0.5$) and its genes were therefore eliminated from the pool.

As witnessed in Figure 3-15 the genetic algorithm with the linear swimming parameter produced certain runs that were described by low thrust but high modified efficiency. Despite these high efficiencies, which occasionally exceeded $\eta_m = 90\%$, the swimming styles that produced them did not survive due to their poor capability for self propulsion at the nominal running speed of 0.6m/s. Nevertheless, their existence stimulated some curiosity and triggered further investigation. Their sporadic appearance across the generations suggested that they were isolated aberrations of the power loss model, a fact that would undermine their credibility. If they could be

68
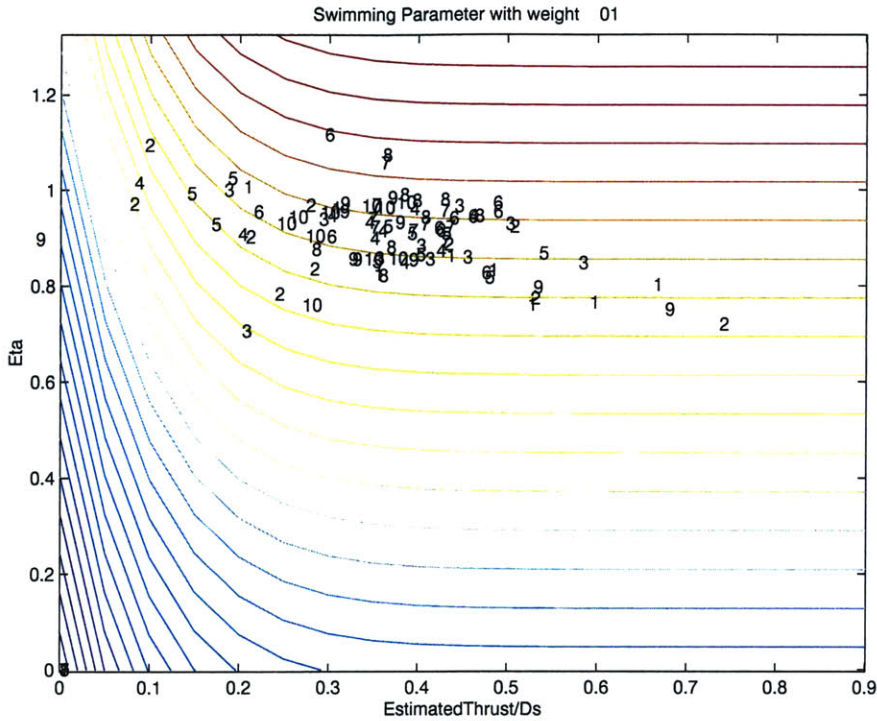
Figure 3-16: Genetic Algorithm intended to investigate low thrust-high efficiency swimming styles.

shown to represent real events however, they would stand as a clear demonstration of the principle of drag reduction.

A new swimming parameter was invented to focus more closely to these "weak" runs and attempt to investigate their validity:

$$SWP = \eta_m - (NDT - 1)^{10}$$

This form was designed to neglect almost completely the issue of self propulsion and place minimal penalty to the non-dimensional thrust, as long as the latter was sufficiently larger than 0. This last condition was necessary to ensure that erratic swimming styles would not prevail. Once again, the efficiency level was not penalized, hoping to detect as much of drag reduction as possible.

The results shown in 3-16 showed that convergence was not reached, which indicated that these super-efficient swimming styles were most probably artifacts of the efficiency calculation. Surprisingly, the aberration was not primarily due to the

power loss model, but due to uncertainty in the thrust measurements. Swimming styles, such as the ones being investigated, which generate very low thrust levels, are plagued with dramatically high relative errors that can easily distort the picture of efficiency. The wrong choice of swimming parameter may therefore allow the genetic algorithm to focus on such styles, which have limited repeatability but also a high probability of producing artificially stellar results. It is to the credit of the linear swimming parameter model being used that such "tempting" aberrations were discarded and their genes failed to survive the generations.

3.4 Recommendations for Future Work

This initial battery of genetic algorithms was marked with some success. Many problems were identified along the way and were partially or completely solved. The rich variety of genetic algorithms and swimming parameter functions is a testimony of the investigative nature of work that took place during the first four months of the new Robotuna's life. Some of the best results obtained from various swimming parameters are summarized in Table 3.3. According to these results, the best propulsive efficiency obtained at self-propelled conditions was slightly less than 40%, significantly lower from what was obtained with the original Robotuna. Furthermore, the apparent richness in the converged parameters shows that optimality is highly dependent on the choice of the swimming parameter. With only a few swimming parameters being used, and just a few genetic algorithms being performed, it should be realized that there is still a vast number of possibilities to be explored. Therefore, dismissing the chance for better results in the near future would be imprudent.

Furthermore, the faulty efficiency indications of the low thrust-producing fish reflect the inherent difficulty in evaluating the efficiency of a structure which produces so little output and is expected of so much! Nevertheless, not only do they not terminate the search for drag reduction, but also they are helpful in describing what the weak points of testing are and essential for suggesting improved testing conditions. For instance, it may be desired to perform a new genetic algorithm based on the linear

SWP type	St	$\alpha(deg)$	$\phi(deg)$	heave(cm)	$\lambda(m)$	$c1 \times 10^5$	NDT	$\eta_m(\%)$	$\eta'(\%)$
line	0.322	20.3	84.1	10.12	1.75	329	0.98	76	36
line	0.322	18.9	85.3	6.02	1.29	6	1.00	73	31
unbiased hyper.	0.332	24.3	90.9	8.84	1.59	373	1.28	X	15
biased hyper.	0.438	21.5	88.5	10.32	1.70	8	1.84	X	15
biased hyper.	0.426	21.7	86.0	10.32	1.70	8	1.79	X	15
biased hyper.	0.332	18.2	88.5	9.28	1.37	170	0.98	X	14

Table 3.3: Summary of some of the best runs obtained from various genetic algorithms. The seven defining parameters include Strouhal number (St), tail-foil angle of attack (α), phase between heave and pitch (ϕ), heave amplitude (in cm), wavelength of body wave (λ in m) and linear profile coefficient (c1).

SWP form, for a higher nominal speed. Increasing the speed would require a parabolic increase to the necessary thrust for self propulsion, which would subsequently help to reduce the uncertainty level of thrust production as it enters the efficiency calculation. Moreover, turbulent stimulators could guarantee early transition to turbulence, and perhaps a further increase in the level of necessary thrust. At the same time, a tail foil with a larger wetted area could be used, so that the Strouhal number range would be kept reasonably low, thus reducing the effect of uncertain power losses associated with high Strouhal numbers.

A preliminary experiment of this type was carried out inconclusively for two reasons. First of all, the straight drag showed significant fluctuations, possibly caused by sloppily placed turbulent stimulators around the nose that deflected from run to run. Secondly, the large torque requirement for the new tail proved to be too excessive for the system to handle, and vigorous swims were aborted as the joint angles were incapable of tracking the required trajectories. It was presumed that there was something inherently wrong with the tuna and also as a sign of deterioration, but

some investigation and maintenance work showed that this was not the case. Most probably then, the problem could be resolved with a finer tuning of the motor gains. Efforts to obtain better results should be a task for the near future, as they could hide the potential for self-propelled fish with drag reduction capabilities.

Chapter 4

Pressure Measurements of the Flow Around the New Robotuna

4.1 Motivation

A significant step towards the understanding of fish hydrodynamics and the unraveling of the mystery behind the capabilities of fish swimming is the measurement of the flow field around the Robotuna. Visual types of measurements have occurred in the past on the old Robotuna, following analogs from live-fish experimentation. On a more advanced and quantitatively accurate note, Digital Particle Image Velocimetry has been applied. It has the advantage of identifying vortical structures which may not be apparent in more qualitative forms of visualization. Furthermore, it has the capability of describing the flow inside the boundary layer of the tuna, thus assessing whether turbulence prevails or some type of relaminarization takes place to reduce the skin drag. Unfortunately, the method of DPIV confines the testing domain to a very small region (of the order of a few centimeters) and thus meets difficulty in presenting the whole picture of vorticity control in fish hydrodynamics.

Dye visualization, although more crude and restricted to a qualitative level only, offers a more global description of the flow around the tuna, but fails to describe body bound vorticity. Other, more secondary problems, further limit its usefulness, such as diffusion and jet effects as the dye shoots out from its tube. More importantly,

surface wave reflections at moderate to high speeds make it impossible to view the dye, and limit the visualization to a range of speeds that is too low to offer any clear vortical patterns. Housing the camera underwater may solve this problem, but also restricts the view considerably.

A more indirect way of characterizing the flow around the Robotuna calls for a measurement of the external pressure field, as sensed on its skin. Carefully selected pressure information may reveal a lot about the vorticity structure of the field, as the two are connected via the Navier-Stokes equations. Although indirect, this method is beneficial for a number of important reasons. Firstly, it resolves the main difficulty found in dye visualization, which is to detect body bound vorticity. Moreover, it offers a more global picture of the hydrodynamics. Most importantly however, it offers measurements that may be processed in real time and serve as outputs in a feedback control system that could attempt to optimize the swimming style of the Robotuna without the "blind" approach of a genetic algorithm. One might be eager to draw an analogy between this type of measurement and the lateral line found in real fish. The lateral line is a highly sensitive organ, stretching longitudinally along the sides of fish's bodies, and are capable of detecting pressure disturbances. This analogy however will not be pursued much further as it is currently believed that the lateral line does not serve as feedback for efficient swimming, but as a much more involved and complex sonar system for predators and prey, as well as guidance for schooling. Although targeted for different uses however, it emphasizes the usefulness of pressure readings as a natural means for underwater sensing. Nevertheless, the term has been borrowed in the context of the Robotuna.

An inherent difficulty of the pressure measurements as a means to describe vorticity is that their effect is not localized. An accurate flow description theoretically requires knowledge of the entire pressure field that surrounds the Robotuna, which is of course impossible to obtain. The task of accurate and quantitative description is therefore very challenging. Despite this difficulty, it may still be possible to identify vortical structures of interest that may be actively involved in the efficiency generating mechanism of the tuna. At the same time, it may be possible to address the

issue of turbulence versus relaminarization by attempting to detect turbulent pressure fluctuations, or even identify possible regions of flow separation. Clever filtering of the pressure signatures could indeed separate the relatively low-frequency, large-scale vortical patterns associated with active voriticy control from the high-frequency, low strength tumbling and bursting mechanism of turbulence. For the current, preliminary state of being, the issue of relaminarization and accurate rectification of the vortical skeleton of the flow was set aside, and all efforts were concentrated on the detection of large structures. As a first step, even a qualitative detection is very useful and may prepare the ground for a more "intelligent" fish that may be aware of its effect on the flow.

4.2 Design Alternatives and Other Considerations

As a first step, it was decided to ignore complicating three-dimensional effects and concentrate on the pressure signature along the lateral line of the Robotuna. Two linear pressure sensor arrays were envisaged, located symmetrically along both sides of the fish. Their exact distance from the nosecone was considered as an issue of low importance for the initial set of experiments, but it was generally agreed to cover mainly two regions, one close to the nose and the other close to the tail. The former is essential for early external vorticity detection, which may subsequently lead to active control in real time. The latter is thought to be useful for educational reasons, as most of the fish's activity occurs near the tail. The grid of the arrays was another parameter that was left for future optimization. With a certain degree of arbitrariness, it was decided that sensor spacing of less than one inch would be very impractical for mounting reasons, as the ribs of the skeletal structure were separated by this amount (not accounting of course for the reduction in spacing which is due to the bending of the body). Moreover, a distance of more than a few inches might present difficulty in monitoring the path of individual vortices as they propagate from nose to tail. In general, smaller distances imply better correlations between sensors, higher confidence in describing the flow, and better "resolution" of the pressure char-

acteristics of the flow. For these reasons, a nominal spacing of 2 inches per sensor was applied. Consequently, an initial double array of 12 sensors was considered to be sufficient, but room was allowed for 24, if a more detailed characterization was deemed important in the future. The possibility of a continuous pressure array strip with optical measurement capabilities would perhaps be a more ideal solution to this problem. Unfortunately, this technology has not reached a stage of maturity yet and cannot be used. Future modifications however should consider this possibility.

The exact method of pressure measurement along this artificial lateral line was a subject of substantial debate. Several options were considered, all of which can be classified in two main categories. The first category called for the installation of the pressure transducers directly on the lateral line, to ensure that the measurements were as real as possible. The second group, was the antithesis of the first one, and allowed for non-collocated sensors that could be safely installed away from the point of application, and would be somehow connected to it by means of a dynamically simple structure.

The main advantage of the first category was that the measured signals would be uncorrupted by any kind of noise or external dynamics (except for the unavoidable sensor noise). Technically speaking then, after some high frequency filtering these signals would be ready to use for the decoding of the vortical skeleton structure. On the other hand, the decision of keeping the sensors on the skin would imply significant problems of practical importance. For instance, the size of the sensors and their necessary external circuitry was thought to be a major issue, given that they would have to hide between the ribs of the Robotuna, which allowed for a total transverse spacing of less than 1 inch. Furthermore, mounting was equally dreaded as an impossible task, due to the thin and soft outer skin that had to remain smooth under stretching and shrinking. Finally, this decision would necessarily imply that the sensors and their attached electronics would have to be fully water-resistant. This feature, in combination with the small size would most probably lead to forbiddingly expensive sensors and would raise the concern of flooding and water-induced corrosion in the near future. The possibility of enclosing all the electronics in underwater,

76

waterproof housings seemed even more remotely difficult, and was considered as an invitation to disaster.

Non-collocated sensing was considered primarily as a direct solution to the difficulties in mounting, water-tightness and space. With the pressure sensors and their related electronics safely above the surface of the water, this alternative stumbled only on the way of communicating the relatively weak pressure signals from the points of application to the receiver ports of the pressure transducers, an overall distance of approximately one meter. The most convenient way of approaching this issue would be to use flexible tubing to enclose a certain fluid medium (most likely air or water) that would offer a bridge between the two points. With separate tubes originating from a central cluster of pressure sensors and stretching to different points on the tuna surface, this system would bear some vague resemblance to the nervous system of a living organism. A major drawback of this method though would be the likely distortion of the original pressure signals during its propagation along the tube. This distortion will be discussed shortly in more detail and is considered to be mainly an outcome of signal attenuation and phase shift due to the inevitable dynamical intervention of the contained fluid in the tubes.

The intuitive thought that short tubes would distort the pressure signals by a lesser amount, raised a new suggestion as a compromise between the two extremes described above. More specifically, it was proposed to mount the sensors at convenient underwater locations near the solid bulkheads (or even inside the nosecone which could be made water-tight), thus resolving the issue of space, avoiding most of the difficulties in mounting and providing some level of water-resistance while reducing the effect of unwanted tube dynamics.

Of all these options, the fully external, non-collocated case was the preferred candidate. Probably the most conservative option, this candidate was chosen over the direct mounted case for reasons of simplicity. The hybrid option of non-collocated underwater sensors was dismissed because it failed to eliminate the effect of tube dynamics, while introducing some of the complications that were inherent to the first method.
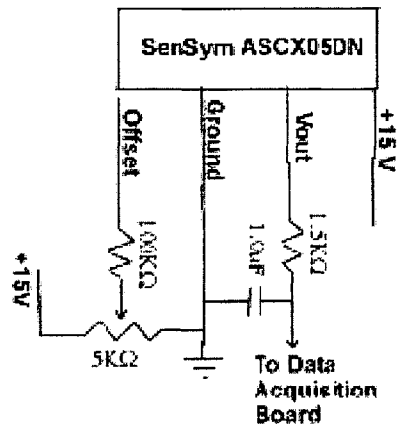
Figure 4-1: Circuit diagram for the ASCX05DN pressure sensor unit.

The pressure sensors were chosen to be the signal conditioned, 0-5psi, Solid State units from SenSym (ASCX05DN). These are robust but inexpensive diaphragm sensors, capable of measuring differential pressure signals. This is a highly desired feature, considering that only pressure fluctuations are necessary for this application. For practicality reasons, the reference pressure was chosen to be the ambient atmospheric, slightly above the surface of the water, where the sensors were located. Thus, in reality the pressure differential includes a hydrostatic component, which amounts to approximately 0.05 bar. This component however may be eliminated by wiring an external potentiometer to offset the nominal voltage. For further noise reduction and signal conditioning, the output signal was passed through a simple, external low pass filter, as shown in Figure 4-1. This filter had a break frequency of around 100Hz, which was safely above the range of frequencies that were expected to represent large scale vorticity.

The pressure sensors were neatly packaged on the vertical hydrofoil mast of the Robotuna, approximately one foot above the water level, where they were protected
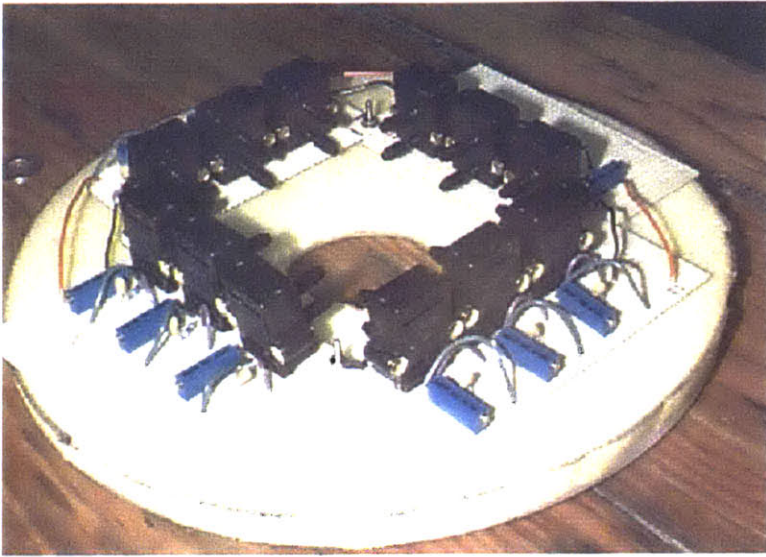
78

Figure 4-2: Cluster Array of 12 Pressure Sensors.

from splashing, while keeping the length of the tubes as short as possible. Arranged in a square formation, they perimetrically surrounded and faced the mast, and where thus able to send their attached flexible tubes through the hydrofoil to the chosen points of application on the skin. A picture of this arrangement is shown in Figure 4-3. The tubes were chosen to be semi-flexible nalgene tubes, 1/8 inches in internal diameter, and 1/4 inches externally. This size proved to be a good compromise between the need to keep a thin bundle that could fit inside the vertical mastpiece, and the effort to reduce signal attenuation, which is a strong function of the inner cross-sectional area. Moreover, a "thick" wall of 1/16 inches was deemed necessary to prevent the tubes from kinking, which would be catastrophic for the propagation of the pressure signals. Inside the fish, the tubes had considerable space to fan out and distribute to the specified skin positions. This, of course, was due to the complete absence of flesh from the new tuna design, and due to the design of a less bulky skeleton that substituted the wide bulkheads of the old Robotuna. Finally, the output signals of the sensors were directed to the main computer board and were subsequently sent directly to the data acquisition system.
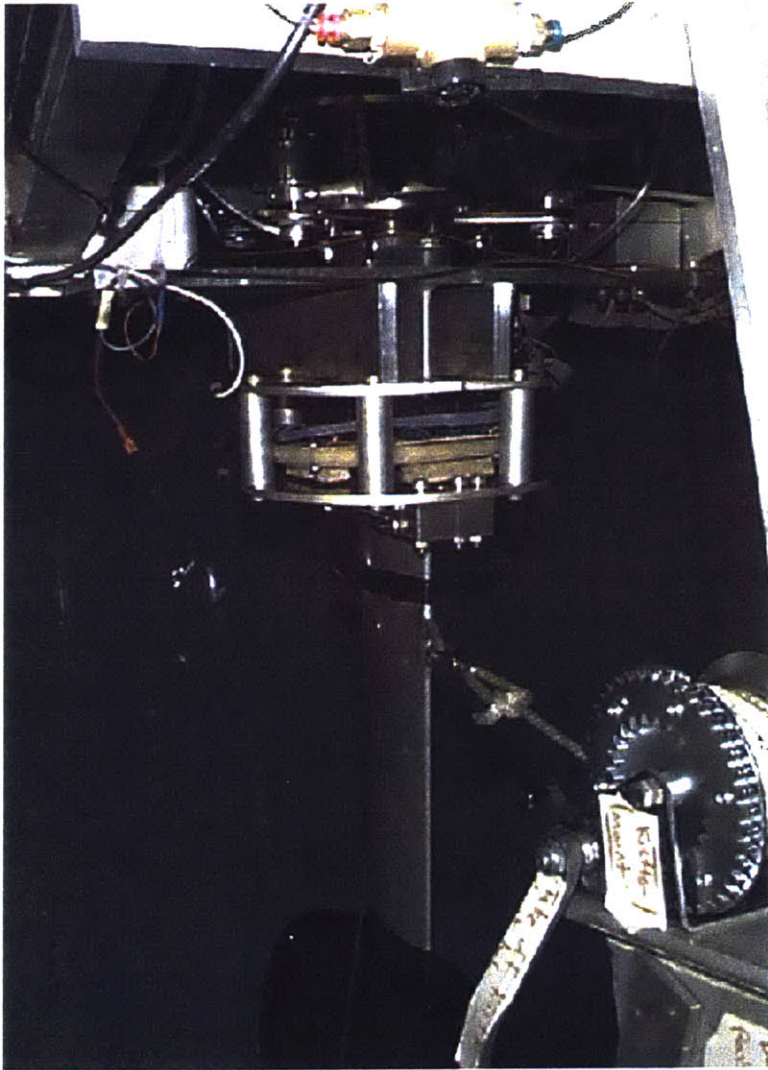
Figure 4-3: Arrangement of cluster of pressure sensors on the mast of the tuna. Nalgene tubes run through the mast and into the fish.

4.3 Tube Dynamics

4.3.1 Modeling of the Dynamic Effects of tubing

Having made the decision to use non-collocated pressure sensing, it was important to determine how the unavoidable tube dynamics affect the pressure signals, what design measures can be taken to reduce this influence, and lastly, how to assess the magnitude of this disturbance. Clearly, if the latter was found to be high, a method of retrieving the original signals from the distorted ones would have to be employed. If the disturbance was classified to be low however, it could be ignored completely and still produce an acceptable picture of the vorticity skeleton structure.

The tube dynamics were modeled as a linear, discrete system of masses, springs and dampers, representing the inertia of the entrained fluid, its compressibility and its skin frictional damping associated with the walls of the tubes. Furthermore, the model assumed that the entrained fluid was a heterogeneous mixture of two substances (air and water) connected together in a "series" formation. This was assumed for the following simple reasons: an air bubble, of some minimum size depending on the magnitude of the largest pressure fluctuations, would have to be maintained near the side of the pressure sensor port, to protect the sensor from contact with water. Since the sensors are not water-tight, such contact might cause degradation of the pressure signal, or even destroy the sensors! Moreover, a certain quantity of water would unavoidably enter the lower part of the tubes, due to the compressibility of the air. Thus, it is very sensible to treat the overall system as a segmented two-fluid system and to try to optimize the relative size of each fluid column.

The linear dynamic model then takes the form shown in Figure 4-4. In this diagram, F represents the pressure force imposed on the edge of the tube, while k_a, c_a and k_w, c_w represent the stiffness and damping caused by the air and water columns respectively. Finally, the boundary condition on the side of the pressure sensor is simply described by a diaphragm with stiffness k_d. It is understood that k_d is significantly larger than the stiffness of air.

This simplistic model is clearly too crude to offer great accuracy in the governing
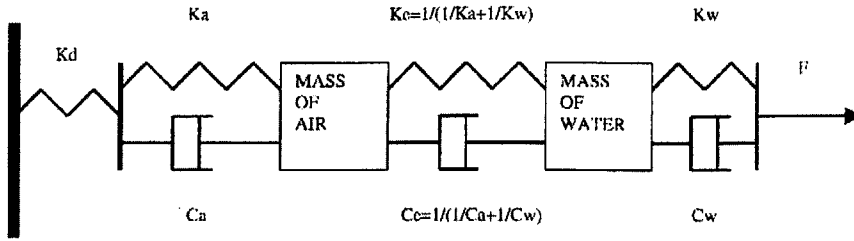
Figure 4-4: Schematic block diagram describing the main components that participate in the tube dynamics.

equations of the tube dynamics, but may be sufficient to mark useful trends and thus help in the design decisions. For instance, it is of utmost importance to predict the natural modes of the system. Signals with frequencies around these modes may resonate and thus produce highly amplified outputs with phase shifts. Furthermore, it is expected that for higher frequencies the tube dynamics may cause severe attenuation. Ideally then, the tube connections should be designed so that their lowest mode is at least twice as large as the highest frequency of pressure fluctuations that might be of use for the decoding of large scale vorticity.

Among the many simplifying assumptions, it is understood that any motion or flexing of the tube may be ignored, the flow has a simple parabolic profile at any given cross-section and any given time, and surface tension effects may be neglected altogether. Further than that, it is assumed that the diaphragm may be modeled as a rigid wall since it has a large stiffness. Mathematically, the approximation may be described as

$$\frac{1}{k_d} + \frac{1}{k_a} \approx \frac{1}{k_a}, k_d >> k_a$$

Similarly, it may be argued that

$$\frac{1}{k_w} + \frac{1}{k_a} \approx \frac{1}{k_a}$$

since $k_w >> k_a$. It is not clear if c_w dominates c_a however, so this approximation may not be carried out for the damping term.
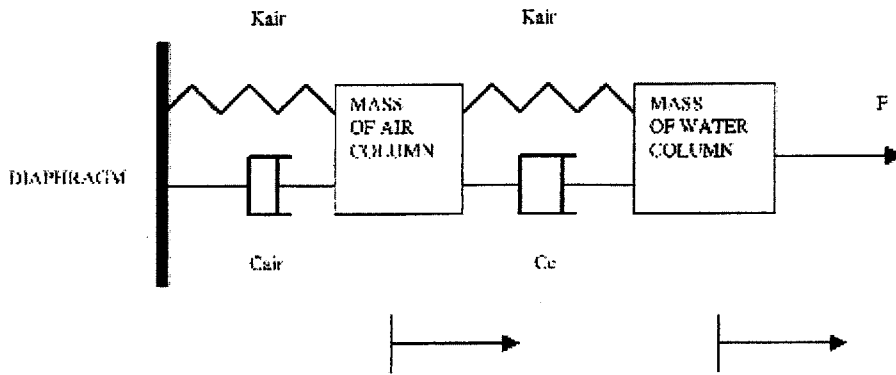
Figure 4-5: Reduced block diagram representation for the tube dynamics.

With all these approximations the initial dynamic model description may be reduced to what is shown in Figure 4-5. The transfer function then which relates pressure disturbances and motions of the sensor's diaphragm is simply given by

$$\frac{X_1}{F} = \frac{\xi}{(m_a s^2 + \lambda s + 2\xi)(m_w s^2 + \xi) - \xi^2}$$

where

$$\xi \equiv k_a + c_e s$$

$$c_e \equiv \frac{c_a c_w}{c_a + c_w}$$

$$\lambda \equiv c_a \frac{1}{1 + \frac{c_w}{c_a}}$$

Since the mass of the air column is always going to be at least an order of magnitude lower than the mass of the water, and assuming that the frictional coefficients are small so that the system is very lightly damped, this expression may be simplified to

$$\frac{X_1}{F} \approx \frac{1/s^2}{2m_w s^2 + k_a}$$

83

which suggests that the natural frequency of the system can be very low for large water columns. More specifically, by assuming air to be an ideal gas the natural frequency may be expressed as:

$$f_n = \frac{1}{2\pi}\sqrt{\frac{k_a}{2m_w}} \approx \frac{1}{2\pi L}\frac{c}{\sqrt{2\gamma}}\sqrt{\frac{\rho_a}{\rho_w}}\frac{r+1}{\sqrt{r}}$$

The adiabatic constant, γ, the speed of sound in air, c, and the density ratio may be considered to be constant, so the natural frequency is only a function of r, the length ratio of the air column to the water column. When the tubes are almost completely filled with air the natural frequency is kept high, which was expected since this implies a low m_w. Nevertheless, this is also the case when the tubes are mostly filled with water, since in that case the stiffness of the air increases dramatically. When the sizes of the air and water columns are equal, the natural frequency reaches its minimum, which can be calculated to be of the order of 1Hz. Clearly, this is a situation that must be avoided at all costs! A good design must ensure that the fluid inside the tube is mostly air or water, and not a mixture of the two in order to avoid resonance conditions.

The damping terms, c_a, c_w may be modeled very simply by recalling the locally Poiseuille flow approximation. By further assuming that all damping is caused by skin friction along the walls of the tube, a simple analysis can be carried out to show

$$\begin{aligned}
c_a &= 8\pi\mu_a L\frac{r}{r+1} \\
c_w &= 8\pi\mu_w L\frac{1}{r+1} \\
\frac{c_a}{c_w} &= \frac{\mu_a}{\mu_w}r
\end{aligned}$$

This shows that even though the dynamic viscosity of water is much larger than the one of air, a large volume ratio, r, prohibits the approximation $c_e \approx c_a$. Furthermore, to minimize the effect of damping losses (which would result in signal attenuation) it seems that c_e has to be maximized, since it is inversely proportional to the power loss for a specified pressure fluctuation. This of course suggests that c_a and c_w must

84

be of the same order of magnitude, which can be interpreted as $r \approx \frac{\mu_w}{\mu_a}$, or $r \gg 1$. For this reason it was chosen to keep the tubes as air-filled as possible.

4.3.2   Testing of the Model

To test the validity of the model described above, a series of pressure tests were performed on the old Robotuna. More specifically, tubes of different size, length, wall thickness, material and enclosed fluid were externally mounted on the tuna, a few inches before the tail region and their results were compared for the same swimming style. This style was chosen arbitrarily, as no attempt to investigate the capabilities of fish swimming was made. Spectral plots where then produced to compare the frequency content of each case, and perhaps detect resonance or damping distortions due to the tube dynamics.

Even though the measured signals seemed to be plagued by a considerable noise level, certain trends could be distinguished well and were found to agree with the analysis described in the previous section. This noise was attributed to some extent to the "clumsy" mounting of the tubes to the body of the tuna. At a nominal speed of 1m/s, the pressure signals were shown to have different frequency spectra depending on the type of entrained fluid in the tubes. In the case of air-filled tubes, two main frequency peaks were detected that corresponded to the undulating frequency of the tuna and perhaps to a first harmonic. This is demonstrated in the frequency spectrum plot in Figure 4-6. When the tubes were mostly water-filled, a strong peak near 6.5Hz was detected, as shown in Figure 4-7. By estimating the ratio of the air to water column, and applying it to the simple model that was discussed previously, this peak was found to be the resonant frequency of the water-filled tube dynamics.

Other runs showed significant signal attenuation for very flexible, thin tubes that were likely to form kinks. Increasing length also played a critical factor in signal attenuation, as did smaller diameters.

As a result of these experiments, it was decided that 1/8 inch Nalgene tubing with a wall of 1/16 inches yielded the best results.
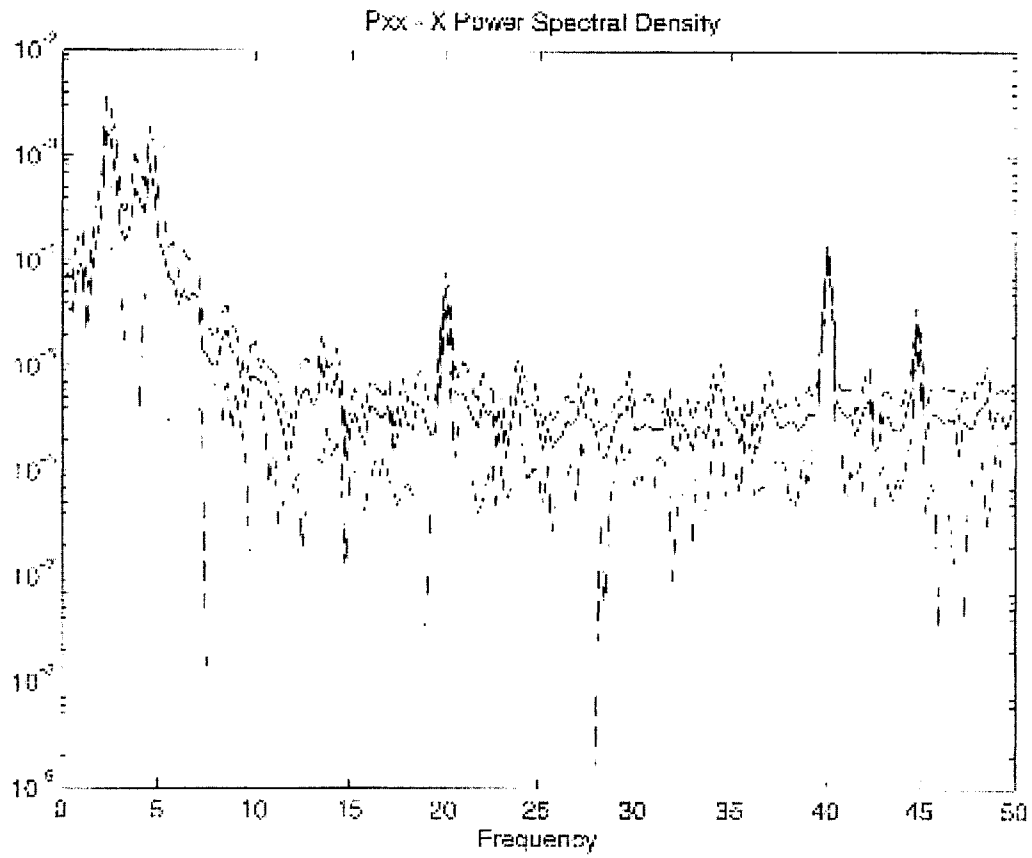
Figure 4-6: Frequency spectrum of pressure trace when the tubes are filled mostly with air.
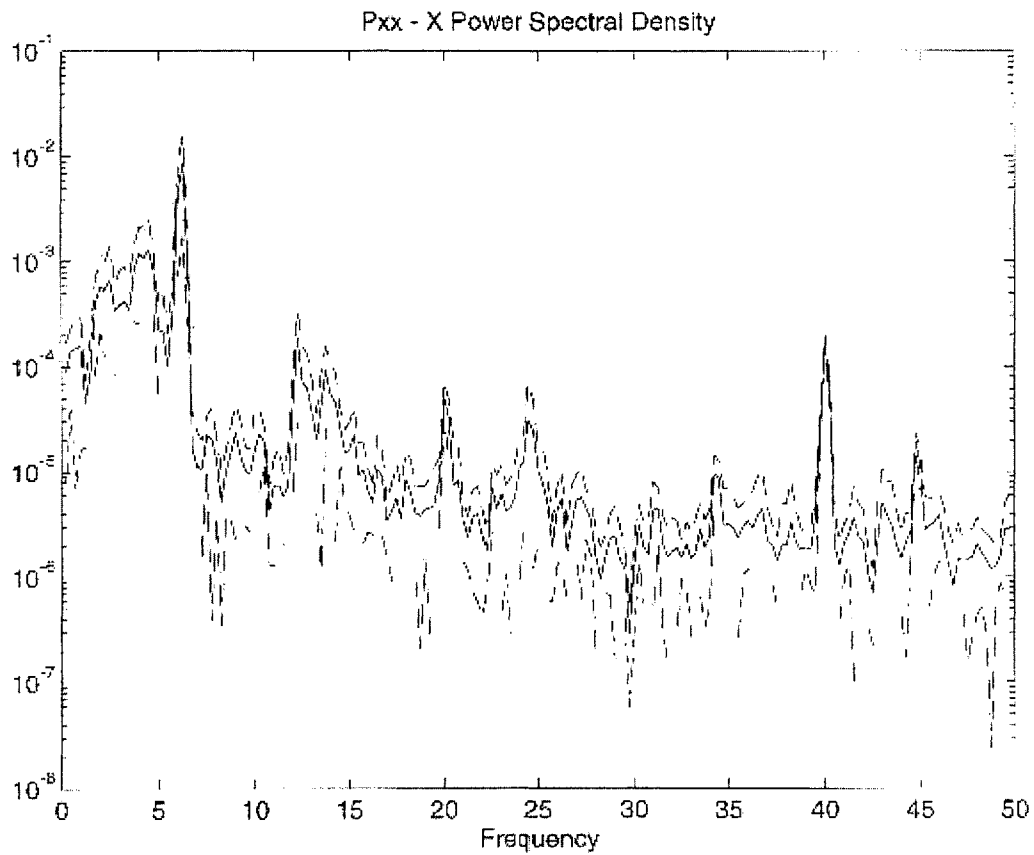
Figure 4-7: Frequency spectrum of pressure trace when the tubes are filled mostly with water.

4.4 Future Pressure Tests on the Robotuna

With the assembly of pressure sensors complete, the ground is now prepared for some initial pressure measurements of the flow around the swimming Robotuna.

Concurrently with the preparation of the sensor assembly, a vortex generator was constructed in the form of a 6-inch, D-shaped aluminum cylinder. This cylinder was designed to be placed vertically at a small distance in front of the nosecone of the tuna (typically 3 to 7 diameters), towed at the nominal carriage speed and swayed slightly to modulate the vortex shedding to a well-defined pattern. The detection of its characteristic Vortex Karman Street wake by the Robotuna's pressure sensors, is targeted as the first goal towards the rectification of a vorticity field through pressure.

Subsequent genetic algorithms are scheduled to investigate optimal swimming styles in the presence of the strong Vortex Karman Street and to relate this optimality to the Robotuna's manipulation of vorticity as seen through pressure.

These tests are expected to be performed in June 2000.

Chapter 5

Concluding Remarks

This thesis has described in some detail a large part of the work that has been conducted on the new Robotuna, from the initial moments of its conception, to the genetic algorithm tests and the introduction of pressure sensors to measure the flow around it. This is by no means an autonomous effort, but merely constitutes a small, intermediate step in a large struggle towards the understanding of the fundamentals of fish swimming. It is therefore hoped that this document will be treated as a clear reference to what has already been accomplished, and as a guide towards further work on the subject.

Bibliography

[1] David S. Barrett. The design of a flexible hull undersea vehicle propelled by an oscillating foil. Master's thesis, Massachusetts Institute of Technology, 1994.

[2] David S. Barrett. *Propulsive Efficiency of a Flexible Hull Underwater Vehicle.* PhD thesis, Massachusetts Institute of Technology, Cambridge, MA, 1996.

[3] Lienhard Beckwith, Marangoni. *Mechanical Measurements.* Addison-Wesley Publishing Company, fifth edition, 1995.

[4] C.C.Lindsey. Form, function, and locomotory habits in fish. In D.J.Randall W.S.Hoar, editor, *Fish Physiology*, number 7, pages 1–88, New York, 1978. Academic Press.

[5] James Gray. *Animal Locomotion.* Weidenfield and Nicolson, London, 1968.

[6] M.J.Wolfgang IV. *Hydrodynamics of Flexible-Body Swimming Motions.* PhD thesis, Massachusetts Institute of Technology, Cambridge, MA, 1999.

[7] Michael V. Jakuba. Deisgn and fabrication of a flexible hull for a bio-mimetic swimming apparatus. 2000.

[8] John M. Kumph. Maneuvering of a robotic pike. Master's thesis, Massachusetts Institute of Technology, 2000.

[9] G. V. Lauder. Function of the caudal fin during locomotion in fishes: Kinematics, flow visualization, and evolutionary patterns. *American Zoologist*, expected 2000.

[10] M. J. Lighthill. Aquatic animal propulsion of high hydrodynamic efficiency. *G-Animal's Journal*, 44:265–301, 1970.

[11] et al. M.W.Westneat. The horizontal septum: Mechanisms of force transfer in locomotion of scombrid fishes (scomgridae,perciformes). *Journal of Morphology*, 217:183–204, 1993.

[12] W. Hill P. Horowitz. *The Art of Electronics*. Cambridge University Press, second edition, 1993.

[13] K.M.Marshek R.C. Juvinall. *Fundamentals of Machine Component Design*. John Wiley and Sons, second edition, 1991.

[14] Sharp and Dizon. *The Physiological Ecology of Tuna*. Academic Press, 1978.

[15] T.J.Pitcher. *The Behavior of Teleost Fishes*. The John Hopkins University Press, Baltimore, Maryland.

[16] Samuel W. Tolkoff. Robotics and power measurements of the robotuna. Master's thesis, Massachusetts Institute of Technology, 1999.

[17] E.J.Stamhuis U.K.Muller, B.L.E. Van Den Heuvel and J.J.Videler. Fish foot prints: Morphology and energetics of the wake behind a continuously swimming mullet. *Journal of Experimental Biology*, 200:2863–2906, 1997.